Study of velocity centroids based on the theory of fluctuations in position-position-velocity space

D. Kandel, A. Lazarian, D. Pogosyan

Monthly Notices
of the
ROYAL ASTRONOMICAL SOCIETY

MNRAS **464,** 3617–3635 (2017)
Advance Access publication 2016 October 3

doi:10.1093/mnras/stw2512

Study of velocity centroids based on the theory of fluctuations in position–position–velocity space

D. Kandel,[1,2]★ A. Lazarian[3]★ and D. Pogosyan[1,2]★

[1] *Physics Department, University of Alberta, Edmonton, AB T6G 2E1, Canada*
[2] *CNRS and UPMC, UMR 7095, Institut d'Astrophysique de Paris, F-75014 Paris, France*
[3] *Department of Astronomy, University of Wisconsin, 475 North Charter Street, Madison, WI 53706, USA*

Accepted 2016 September 30. Received 2016 September 6; in original form 2016 July 14; Editorial Decision 2016 September 29

ABSTRACT

We study the possibility of obtaining power spectrum of gas velocity in the turbulent interstellar medium from spatial correlation of velocity centroids (VCs) of optically thick emission lines. Combining this study with the earlier studies of centroids in Esquivel & Lazarian, we conclude that centroids are applicable for studies of subsonic/transonic turbulence for sufficiently small line-of-sight (LOS) separations at which self-absorption does not affect correlation scalings. At larger LOS separations where self-absorption becomes important, we find that there is a range of scales over which VC correlation demonstrates the universal scaling, similar to the effect found in the velocity channel analysis (VCA). In other words, for large absorptions the VCs lose their ability to reflect the spectra of turbulence. We develop analytical formalism that relates statistical properties of underlying magnetohydrodynamical (MHD) turbulence to observable scaling and anisotropy of VC correlations arising from Alfvén, slow and fast modes that constitute the compressible MHD modes, and show how the VC anisotropy can be used to find the media magnetization as well as to identify and separate the contributions from these MHD modes. Our study demonstrates that VCs are complementary to the VCA. In order to study turbulent volume with insufficient resolution of single-dish telescopes, we demonstrate how the studies of anisotropy can be performed using interferometers. We also suggest that restricted VC can be constructed for absorption lines by integrating LOS velocity weighted by the optical depth. We discuss the requirements for applicability of this approach.

Key words: magnetic fields – turbulence.

1 INTRODUCTION

The interstellar medium (ISM) is magnetized and turbulent. Observations of non-thermal Doppler broadening of spectral lines, fluctuations of density and synchrotron emission (see reviews by Cho, Lazarian & Vishniac 2003; Elmegreen & Scalo 2004; Mac Low & Klessen 2004; Ballesteros-Paredes et al. 2007; McKee & Ostriker 2007; Lazarian 2009) are some cases that suggest the ubiquity of magnetohydrodynamic (MHD) turbulence in the ISM. Moreover, the estimated Reynolds number in the ISM is of the order of 10^8, suggesting turbulent flows which are possibly driven by various causes such as supernova explosion and magnetorotational instabilities (Mac Low & Klessen 2004). Thus, MHD turbulence is of key importance for star formation (Federrath & Klessen 2012; Federrath 2013; Salim, Federrath & Kewley 2015), propagation and acceleration of cosmic rays and other fundamental astrophysical processes (see Brandenburg & Lazarian 2013 and references therein).

Understanding the interstellar turbulence requires one to successfully study the statistics of underlying turbulent field, in particular to obtain the velocity and density spectrum of the turbulent field. One of the frequently used techniques to obtain velocity spectra using spectral lines is velocity centroids (VCs), which are first moments of spectral line (see Münch & Wheelon 1958; Kleiner & Dickman 1985; O'dell & Castaneda 1987; Miesch, Scalo & Bally 1999). Esquivel & Lazarian (2005) studied the extent up to which VCs correctly reflect the turbulence velocity spectrum. Numerical studies (see Esquivel & Lazarian 2005; Esquivel et al. 2007) have later shown that the spectrum can be obtained adequately correctly for subsonic turbulence, but is significantly distorted for supersonic turbulence. The former property of VC was found to be complementary to the properties of the two more recent techniques based on the analytical description of turbulence, namely, velocity channel analysis (VCA; Lazarian & Pogosyan 2000, 2004, hereafter LP00 and LP04, respectively) and velocity coordinate spectrum (VCS; Lazarian & Pogosyan 2006, 2008, hereafter LP06 and LP08, respectively). The findings of those papers suggest that studies of subsonic turbulence are possible only for heavier species moving with the flow, e.g. heavy ions, atoms and molecules moving together

★ E-mail: dkandel@ualberta.ca (DK); alazarian@facstaff.wisc.edu (AL); pogosyan@ualberta.ca (DP)

with atomic or molecular hydrogen. The analytical description that was at the core of the VCA and VCS techniques made them advantageous compared to VCs, which were studied only numerically.

The VCA technique has been successfully tested and elaborated in a number of subsequent papers (Lazarian et al. 2001; Chepurnov & Lazarian 2009; Burkhart et al. 2013) and was successfully applied to a number of observations (see an incomplete list in Lazarian 2009). In terms of the spectra study, the VCA technique suggests a way of disentangling velocity and density contributions to the channel maps through varying the thickness of the corresponding maps. This technique has been successfully applied to H I and CO data in e.g. Padoan et al. (2009), Chepurnov & Lazarian (2010) and Chepurnov et al. (2015) to obtain velocity spectra.

Velocity and density spectra do not provide a complete description of an underlying turbulent field, particularly in a magnetized plasma. MHD turbulence is known to be anisotropic with magnetic field defining the direction of anisotropy (Montgomery & Turner 1981; Shebalin, Matthaeus & Montgomery 1983; Higdon 1984). In this regard, apart from spectra, the direction of magnetic field and magnetization can also be studied with the position–position–velocity (PPV) data. The first demonstration of this possibility of obtaining magnetic field direction was given in Lazarian, Pogosyan & Esquivel (2002), which was followed by the subsequent empirical studies in this direction (e.g. Esquivel & Lazarian 2011; Burkhart et al. 2014). The research based on analytical studies was carried out not with spectroscopic, but synchrotron data. Lazarian & Pogosyan (2012, 2016, hereafter LP12 and LP16, respectively) carried out the analytical description of synchrotron intensity and polarization fluctuation for the model of turbulence containing Alfvén, fast and slow mode cascades (see Brandenburg & Lazarian 2013 and references therein). The analytical description of anisotropies in LP12 and LP16 allowed us to relate the analytical predictions of magnetization of the media and the observed anisotropy of the synchrotron polarization and intensity fluctuations. The approach in these works was used in Kandel, Lazarian & Pogosyan (2016, hereafter KLP) to provide the analytical description of the anisotropies in PPV space, extending the VCA in the case of anisotropic turbulence. The study in KLP provides the foundation for our present study of anisotropy using VC. The use of VCs for studying the turbulence anisotropy and thus determining the direction of magnetic field with spectroscopic data was suggested and elaborated in Esquivel & Lazarian (2005, 2011) and Burkhart et al. (2014). The numerical simulations in those works showed this to be a powerful technique for studying media magnetization. However, the technique stayed empirical in that sense being similar to its counterpart that uses principal component analysis (PCA; Heyer & Peter 1997). In this paper, we provide a theoretical study of turbulence anisotropies using VCs.

In this paper, we aim to present a comprehensive study of VCs by extending centroids to study turbulence in a self-absorbing medium, as well as with absorption lines. We also present a formulation of centroids anisotropy in order to study anisotropy of an underlying MHD turbulence. The structure of our paper is as follows: in Section 2.1, we review important expressions of centroids through PPV space formalism, which we extend in Section 3 to describe the centroid statistics in the presence of self-absorption. In Section 4, we describe the usefulness and limitations of centroids in the case of absorption lines. In Section 5, we develop a general formalism to study turbulence anisotropies through centroids, and we apply this formalism to specific MHD modes in Section 6. In Section 7, we show how interferometric data can be used to study turbulence using centroids technique. The major findings of the paper are summarized in Section 8, and comparisons between VCA and centroids are made in Section 9. The practical issues of turbulence studies using centroids are presented in Section 10. In Section 11, we discuss about the foundation of our technique, the assumptions we used and the range of applicability of centroids; and relate our study with other existing technique. Finally, we summarize our important findings in Section 12.

2 VELOCITY CENTROIDS

The *in situ* point-wise measurements in XYZ space are not available with spectroscopic measurements. Therefore, measurements of the intensity of emissions are defined in PPV space or XYV volume, where the turbulence information along the z-axis is subject to a non-linear transformation due to the mapping to the line-of-sight (LOS) velocity axis. Doppler shifts are affected only by the LOS (which we assume to be aligned with z-axis) component of turbulent velocities, which to simplify our notations, we denote as v (instead of v_z). All the relevant notations used in this paper are presented in Table A1.

The theory of intensity fluctuations in PPV space was pioneered in LP00 and was later extended for special cases in LP04, LP06, LP08 as well as in the anisotropy studies in KLP. In this paper, we work in PPV space to study how the VCs reflect velocity spectra as well as anisotropic nature of the velocity and density statistics in magnetized turbulence. In this section, we begin to develop framework to study centroids in the presence of self-absorption. For that we first derive the centroid correlation as well as structure function through PPV space. The description of centroids in PPV space turns out to be valuable to understand the effects of self-absorption on centroids.

Before starting formal derivations, we assume turbulence to be homogeneous and isotropic in Sections 2 and 4, while the assumption of isotropy will be relaxed in Sections 5 and 6 to study anisotropies due to magnetization of a turbulent media. Furthermore, we assume that the statistical measures such as structure function and correlation functions of velocity and density fluctuations to obey power-law behaviour on scale, i.e. $\propto r^{-p}$. Fluctuations whose most power is on the large scales are called *steep*, while those whose most power is on the small scales are called *shallow*. A major difference between correlation function and structure function is that, while the structure function at some scale r is determined by the integrated power of fluctuations over scales smaller than r, the correlation function is determined by the integral of the power over scales larger than r. Therefore, the correlation function is more appropriate to use for shallow spectra, while the structure function is more appropriate for steep spectra (Monin, Yaglom & Lumley 1975). Our derivation is based for steep velocity spectra, for which we assume LOS -projected structure function to be of the form $D_z(r) \sim r^{-\nu}$. For shallow density spectra we use $\xi_\rho(r) \sim \langle\rho\rangle^2 + \langle\delta\rho^2\rangle(r/r_c)^{-\nu_\rho}$, while for steep spectra we use $\xi_\rho(r) \sim \langle\rho\rangle^2 + \langle\delta\rho^2\rangle - \langle\delta\rho^2\rangle(r/r_c)^{-\nu_\rho}$, where r_c is the correlation length of the density field. In the case of shallow spectra, the dynamical range exists at $r > r_c$, for steep spectra, the dynamical range exists at $r < r_c$.

The centroid in PPV space is the moment of intensity defined as (see Miesch & Bally 1994)

$$C_N(\boldsymbol{X}) = \frac{\int \mathrm{d}v_1\, v_1 I_{v1}(\boldsymbol{X})}{\int \mathrm{d}v_1\, I_{v1}(\boldsymbol{X})}, \tag{1}$$

where I_{v1} is the spectral intensity and v_1 is the LOS velocity. By solving one-dimensional radiative transfer equation in the case of

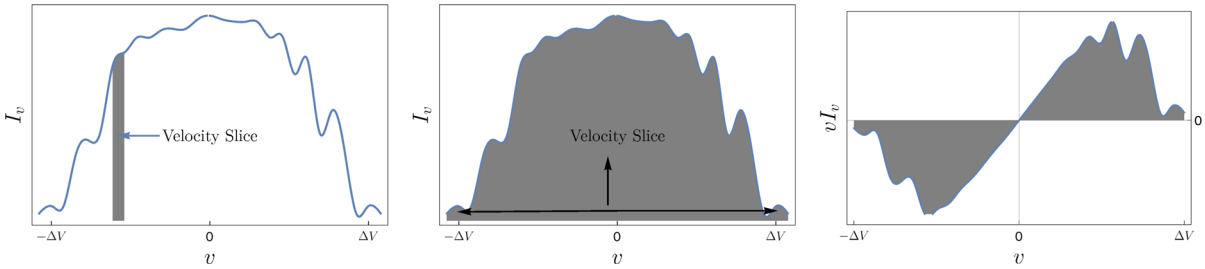

Figure 1. Schematic showing geometrical differences between construction of VCA and of centroids. Left-hand panel: construction of thin-slice VCA. Only channels of thin total velocity width δv need to be used to find the intensity. Central panel: construction of thick-slice VCA. Effectively, integration over the entire line width is carried out to find intensity. Right-hand panel: construction of VCs. Velocity-weighted moment of intensity is constructed and integrated over entire line width.

Table 1. Different types of centroids.

Type of centroids	Definition	Structure function
Normalized centroid	$C_N(\boldsymbol{X}) = \frac{\int \mathrm{d}v_1\, v_1 I_{v1}(\boldsymbol{X})}{\int \mathrm{d}v_1\, I_{v1}(\boldsymbol{X})}$	Not used in this paper
Unnormalized centroid	$C(\boldsymbol{X}) = \int \mathrm{d}v_1\, v_1 I_{v1}(\boldsymbol{X})$	Equation (15)
Modified centroids	Only structure function is defined	Equation (69)
Restricted centroids[a]	Equation (32)	Equation (33)

Note. [a]Restricted centroids are used for saturated absorption lines.

self-absorbing emission in spectral lines, one can obtain the spectral intensity as (see LP04)

$$I_v(\boldsymbol{X}) = \frac{\epsilon}{\alpha}\left[1 - \mathrm{e}^{-\alpha\rho_s(\boldsymbol{X},v)}\right], \tag{2}$$

where ϵ is the emissivity coefficient, α is the self-absorption coefficient, v is the LOS velocity, $\boldsymbol{X}$ is the sky-projected two-dimensional position vector, ρ_s is the PPV space density given by

$$\rho_s(\boldsymbol{X}, v) = \int \mathrm{d}z\, \rho(\boldsymbol{x})\Phi(v - u(\boldsymbol{x})), \tag{3}$$

with $\boldsymbol{x}$ is the three-dimensional position vector of a turbulent point, $\Phi(v - u(\boldsymbol{x}))$ being the Maxwell's distribution of the thermal component of LOS velocity, and $u(\boldsymbol{x})$ being the LOS turbulent velocity.

Due to presence of denominator term in the definition of centroids in equation (1), $C_M(\boldsymbol{X})$ is non-linear function of I, which complicates relation between statistics of centroids and intensity. To remedy this difficulty, Lazarian & Esquivel (2003, henceforth LE03) introduced 'unnormalized' velocity centroids (UVCs) defined as

$$C(\boldsymbol{X}) = \int \mathrm{d}v_1\, v_1 I_{v1}(\boldsymbol{X}). \tag{4}$$

The geometric construction of UVC is presented in the right-hand panel of Fig. 1. A summary of different types of centroids is presented in Table 1. In all the subsequent sections, we carry out analysis with unnormalized centroids.

2.1 Centroids for optically thin emission lines

In this section, we first review unnormalized centroids in the case when self-absorption is negligible. In this case, equation (2) gives

$$I_v(\boldsymbol{X}) = \epsilon\rho_s(\boldsymbol{X}, v), \tag{5}$$

and, therefore equation (4) gives

$$C(\boldsymbol{X}) = \epsilon \int \mathrm{d}v\, v\rho_s(\boldsymbol{X}, v). \tag{6}$$

The usual approach in the study of centroids is to work in position-position-position space rather than PPV space. This can be achieved by writing equation (6) as

$$\begin{aligned} C(\boldsymbol{X}) &= \epsilon \int \mathrm{d}v\, v \int \mathrm{d}z\, \rho(\boldsymbol{x})\Phi(v - u(\boldsymbol{x})) \\ &= \epsilon \int \mathrm{d}z\, \rho(\boldsymbol{x}) \int \mathrm{d}v\, v\Phi(v - u(\boldsymbol{x})) \\ &= \epsilon \int \mathrm{d}z\, u(\boldsymbol{x})\rho(\boldsymbol{x}), \end{aligned} \tag{7}$$

where $\rho(\boldsymbol{x})$ is the real space density and $u(\boldsymbol{x})$ is the z-component of the turbulent velocity.

However, in order to make a smooth connection between the optically thin case and the optically thick case, we derive centroids correlation function by working in the PPV space. This is straightforwardly achieved by utilizing the theory of fluctuations of PPV space density $\rho_s(\boldsymbol{X})$ developed in LP00 and LP04. Using equation (4), the correlation of centroids can be written as

$$\begin{aligned} \xi(\boldsymbol{R}) = &\int_{-S}^{S} \mathrm{d}z_1 \int_{-S}^{S} \mathrm{d}z_2\, \xi_\rho(\boldsymbol{r}) \int_{-\infty}^{\infty} \mathrm{d}v_1\, v_1 \\ &\int_{-\infty}^{\infty} \mathrm{d}v_2\, v_2 \langle \Phi(v_1 - u(\boldsymbol{x}_1))\Phi(v_2 - u(\boldsymbol{x}_2))\rangle, \end{aligned} \tag{8}$$

where $\boldsymbol{R} = \boldsymbol{X}_1 - \boldsymbol{X}_2, \boldsymbol{r} \equiv (\boldsymbol{R}, z) = \boldsymbol{x}_1 - \boldsymbol{x}_2$ and $\xi_\rho(\boldsymbol{r})$ is the density correlation function. In equation (8), $\langle \dots \rangle$ denotes the averaging over turbulent velocity $u(\boldsymbol{x})$ as a random quantity. The main assumption in writing equation (8) is that the density and velocity fields are uncorrelated. This assumption has been tested in the past papers (e.g. Esquivel et al. 2007), and seems to be sufficiently accurate for subsonic turbulence with density dispersion less than the mean density of a turbulent cloud. Assuming that the turbulent velocity is a Gaussian random vector, whose variance of the pairwise difference between two vectors is given by the structure function

$$D_{ij}(\boldsymbol{x}_2 - \boldsymbol{x}_1) = \left\langle \left(u_i(\boldsymbol{x}_1) - u_i(\boldsymbol{x}_2)\right)\left(u_j(\boldsymbol{x}_1) - u_j(\boldsymbol{x}_2)\right)\right\rangle, \tag{9}$$

and the z-projected structure function is given by

$$D_z(\boldsymbol{x}_2 - \boldsymbol{x}_1) = D_{ij}(\boldsymbol{x}_2 - \boldsymbol{x}_1)\hat{z}_i\hat{z}_j. \tag{10}$$

With this, equation (8) reduces to

$$\xi(\boldsymbol{R}) = \frac{1}{2\pi}\int_{-S}^{S} \mathrm{d}z \left(1 - \frac{|z|}{2S}\right) \int_{-\infty}^{\infty} \mathrm{d}v \int_{-\infty}^{\infty} \mathrm{d}v_+ \left(v_+^2 - \frac{v^2}{4}\right) \times \frac{\xi_\rho(\boldsymbol{r})}{\sqrt{D_z(\boldsymbol{r}) + 2\beta_\mathrm{T}}} \exp\left[-\frac{v^2}{2(D_z(\boldsymbol{r}) + 2\beta_\mathrm{T})}\right] \sqrt{\frac{2}{D^+(S,\boldsymbol{r})}} \times \exp\left[-\frac{v_+^2}{D^+(S,\boldsymbol{r})}\right], \tag{11}$$

where

$$D^+(S,\boldsymbol{r}) \equiv \beta_\mathrm{T} + D_z(S) - D_z(\boldsymbol{r})/2, \tag{12}$$

and $D_z(\boldsymbol{r})$ is the z-projected velocity structure function, $\beta_\mathrm{T} \equiv k_\mathrm{B}T/m$ is the thermal broadening, m being the mass of atoms, T being the temperature and k_B being the Boltzmann constant. After performing the integration over v, we finally obtain

$$\xi(\boldsymbol{R}) = \frac{1}{2}\int_{-S}^{S} \mathrm{d}z \left(1 - \frac{|z|}{2S}\right) \xi_\rho(\boldsymbol{r})(D_z(S) - D_z(\boldsymbol{r})). \tag{13}$$

Note that our formalism cleanly shows how thermal effects drop out in centroids upon carrying out the integral in equation (11) to obtain equation (13). This shows that turbulence velocity spectrum can be recovered with centroids regardless of the temperature,[1] which is distinct from other techniques (e.g. VCA).

The centroids structure function is defined as

$$\mathcal{D}(R) = \left\langle [C(\boldsymbol{X}_1 + \boldsymbol{R}) - C(\boldsymbol{X}_1)]^2 \right\rangle. \tag{14}$$

Utilizing equations (13) and (14), we finally obtain the centroid structure function

$$\mathcal{D}(\boldsymbol{R}) \approx \int_{-S}^{S} \mathrm{d}z \left\{ D_z(S)\left(\xi_\rho(0,z) - \xi_\rho(\boldsymbol{r})\right) + [\xi_\rho(\boldsymbol{r})D_z(\boldsymbol{r}) - \xi_\rho(0,z)D_z(0,z)] \right\}. \tag{15}$$

With the assumption of zero correlation between density and velocity, the above result for optically thin line is identical to that obtained in LE03, where the same result was obtained by directly utilizing equation (7). Working from first principles in the PPV space, as is done in this paper, is especially useful to deal with centroids in the presence of self-absorption.

For a constant density field and at $R \ll S$, the centroid structure function is

$$\mathcal{D}(R) \propto R^{1+\nu}, \tag{16}$$

which is the regular centroid scaling. We use this scaling further in this paper.

3 CENTROIDS FOR OPTICALLY THICK EMISSION LINES

With the introduction of centroids in PPV space, the extension of centroids to an absorbing media is straightforward. In this case, using full expression for intensity given by equation (2) in equation (4) yields

$$C(\boldsymbol{R}) = \frac{\epsilon}{\alpha}\int \mathrm{d}v\, v \left[1 - \mathrm{e}^{-\alpha\rho_\mathrm{s}(X,v)}\right]. \tag{17}$$

Using equations (14) and (17) and following LP04, one can obtain

$$\mathcal{D}(R) = \frac{\epsilon^2}{\alpha^2}\int_{-\infty}^{\infty}\mathrm{d}v_1\, v_1 \int_{-\infty}^{\infty}\mathrm{d}v_2\, v_2 \Big\langle \mathrm{e}^{-\alpha(\rho_{11}+\rho_{12})}\Big(1 + \mathrm{e}^{-\alpha(\rho_{22}+\rho_{21}-\rho_{11}-\rho_{12})} - \mathrm{e}^{-\alpha(\rho_{21}-\rho_{11})} - \mathrm{e}^{-\alpha(\rho_{22}-\rho_{12})}\Big)\Big\rangle, \tag{18}$$

where $\rho_{ij} \equiv \rho_\mathrm{s}(\boldsymbol{X}_i, v_j)$. Note that the exponential terms inside the parenthesis are split in such a way that the velocity is the same for two terms that make up a difference. As explained in LP04, the reason for this arrangement is that at small separations R, the terms inside are small and therefore the exponential can be expanded, retaining only the leading order terms. This leads to

$$\mathcal{D} \approx \epsilon^2 \int_{-\infty}^{\infty}\mathrm{d}v_1\, v_1 \int_{-\infty}^{\infty}\mathrm{d}v_2\, v_2 \Big\langle \mathrm{e}^{-\alpha(\rho_{11}+\rho_{12})} \times [(\rho_{11} - \rho_{21})(\rho_{12} - \rho_{22})]\Big\rangle. \tag{19}$$

The above expression is the main expression that we study further. If one assumes density and velocity to be uncorrelated, this expression can be sufficiently simplified. The details of this simplification are presented in LP04. Here, we present the final result

$$\mathcal{D}(\boldsymbol{R}) \propto \epsilon^2 \int_0^S \mathrm{d}z \int_{-\infty}^{\infty}\mathrm{d}v\, \mathrm{e}^{-\frac{\alpha^2}{2}\bar{d}_s(0,v)}[\mathcal{W}(\boldsymbol{R},z,v)d_s(\boldsymbol{R},z,v) - \mathcal{W}(0,z,v)d_s(0,z,v)], \tag{20}$$

where

$$\mathcal{W}(\boldsymbol{R},z,v) = \int_{-\infty}^{\infty}\mathrm{d}v_+ \left(v_+^2 - \frac{v^2}{4}\right)\sqrt{\frac{2}{D^+(S,\boldsymbol{r})}} \times \exp\left[-\frac{v_+^2}{D^+(S,\boldsymbol{r})}\right], \tag{21}$$

and

$$d_s(\boldsymbol{R},z,v) = \frac{1}{\sqrt{D_z(\boldsymbol{r}) + 2\beta_\mathrm{T}}}\exp\left[-\frac{v^2}{2(D_z(\boldsymbol{r}) + 2\beta_\mathrm{T})}\right]. \tag{22}$$

In equation (20), $d_s(\boldsymbol{R},v) = d_v(\boldsymbol{R},v) + d_\rho(\boldsymbol{R},v)$. We focus on the case when velocity term is dominant. Our treatment to obtain equation (20) is valid only when $\alpha^2(d_s(R,v) - d_s(0,v) < 1$ so that non-linear effects are negligible. A simpler, but loose, condition for velocity term is $\alpha^2 d_v(R,0) < 1$. This condition can be formally written by noting that the asymptote of $d_v(R,0)$ is given by $d_v(R,0) \sim R^{1-\nu/2}$, where we have omitted numerical pre-factors that are of the order of unity. Restoring proper dimensionality, one can estimate the scales for which our treatment is applicable and this is given by

$$\alpha^2\langle\rho_\mathrm{s}\rangle^2 < \left(\frac{S}{R}\right)^{1-\nu/2}. \tag{23}$$

If the above condition is not fulfilled, one will see non-linear behaviour of the centroid structure function instead of power law in R. Note that the expression for centroid structure function derived in this paper (cf. equation 20) and intensity structure function derived in LP04 looks similar. Closer inspection shows that the difference comes through the factor $\mathcal{W}(v)$. It is also important to note that the R dependence in the $\mathcal{W}(v)$ given by equation (21)

[1] For very hot plasmas, noise levels can distort centroid statistics. See Section 10 for more clarification.

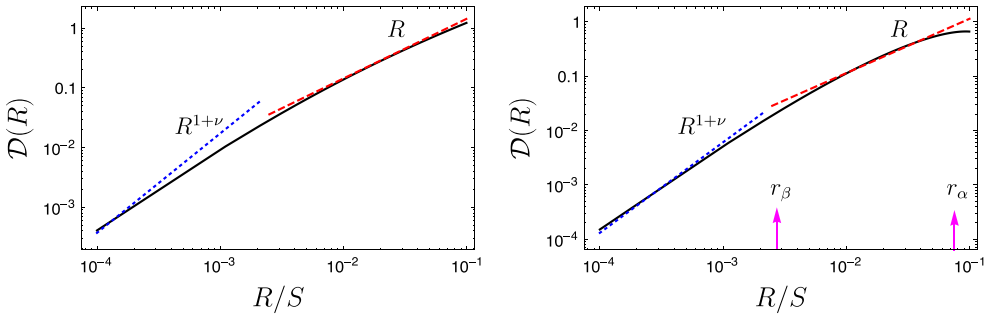

Figure 2. Centroid structure function for different levels of self-absorption for velocity spectrum with Kolmogorov index $\nu = 2/3$ and for constant density field. The left-hand panel is for $\beta_T = 0$, so that $r_\beta \equiv (\beta_T/D_z(S))^{1/\nu} = 0$, and at $r_\alpha \equiv (v_c^2/(D_z(S) + 2\beta_T))^{1/\nu} = 0.2$. The right-hand panel is for different parameters defining thermal broadening and the level of self-absorption r_β and r_α, that are shown clearly in the figure. These panels clearly show two asymptotes scaling described in the text.

is weak, as $\beta_T + D_z(S) - D_z(\boldsymbol{r})/2$ is nearly a constant. For strong self-absorption, non-linear effects are important. In the case of moderate self-absorption, equation (20) can be written as

$$\mathcal{W}(\boldsymbol{R}, z, v) = \sqrt{\frac{\pi}{2}}\left(\beta_T + D_z(S) - \frac{D_z(\boldsymbol{r})}{2} - \frac{v^2}{2}\right). \quad (24)$$

The main effect of absorption is the introduction of an exponentially suppressing factor $\exp[-\alpha^2\tilde{d}_s(0, v)/2]$. This is effectively a window, which tells us how integration over v should be carried out. The critical width of absorption window is given by

$$\alpha^2 d_s(0, v_{ab}) = 1. \quad (25)$$

The effects of absorption become strong for $v > v_{ab}$. Note that for weak self-absorption, i.e. for small α, v_{ab} is large and vice versa. Taking into consideration, the power-law behaviour of velocity structure function and density correlation function, one can solve for asymptotes of $d_s(0, v)$ to obtain (see LP04 for details)

$$v_{ab} \approx \sqrt{D_z(S) + 2\beta_T}(\alpha\bar{\rho})^{\frac{2\nu}{\nu-2(1-\nu_\rho)}}, \qquad \nu > (2/3)(1-\nu_\rho) \quad (26)$$

$$v_{ab} \approx \sqrt{D_z(S) + 2\beta_T}(\alpha\bar{\rho})^{-1}, \qquad \nu < (2/3)(1-\nu_\rho), \quad (27)$$

where the mean density $\bar{\rho} = \langle\rho_s\rangle(D_z(S) + 2\beta_T)^{1/2}/S$. Equations (26) and (27) are valid only when absorption is moderate so that $\alpha\bar{\rho} < 1$.

At this point, we ask the following question: in the presence of absorption, can the velocity spectra be recovered? The subsequent analysis in this section is focused to answer this question. Before we start, we would first like to make some remark on the VCA technique developed in LP00 and LP04, because some of the asymptotes of the centroid structure function in the presence of self-absorption will be similar to that in VCA. The VCA was developed for intensity (unlike centroids where we multiply LOS velocity and intensity). In VCA, one can control thickness of velocity slice from which data are analysed (see LP00 and LP04). In a thin-slice regime, the velocity window is essentially a delta function, and one can see the effects of turbulence velocity on intensity in this regime. In fact, a small-scale asymptote of pure velocity contribution to the intensity structure function follows the scaling $R^{1-\nu/2}$, which is the thin-slice asymptote. On the other hand, for thick slice in an optically thin media, one essentially integrates over the entire range of velocity with a flat function, and in this regime velocity effects are erased and only density effects are manifested. It is important to note that to produce 'thin-slice' asymptote, the velocity cut-off introduced by the window has to be less than $\sqrt{D_z(\boldsymbol{R})}$.

The whole point of the above review of the VCA is the following: although centroids are for integrated lines (and thus notion of 'slice thickness' does not exist), self-absorption introduces an 'effective slice thickness'. In fact, when self-absorption is large, both centroids and VCA yield the same 'thin-slice' result. This can be seen from equation (11), and noting the fact that $\beta_T + D_z(S) - D_z(\boldsymbol{r})/2$ is nearly a constant. In the case when self-absorption is negligible, centroids are defined effectively in 'thick-slice' limit (as there is no window in the definition of centroids), and therefore this 'thin-slice' asymptote can never be realized. The situation is different in the presence of self-absorption, as the factor $\exp[-\alpha^2 d_s(0, v)/2]$ in equation (20) introduced by self-absorption effectively acts like a window. Therefore, it is natural to expect that there exists a regime where even centroids produce 'thin-slice' regime, which was relevant in the VCA.

In the case when $\nu \geq 2/3$, one can combine equations (26) and (23) to obtain the condition for the validity of linear expansion $v_{ab}^2 \geq (D_z(S) + 2\beta_T)(R/S)^\nu$, meaning that the critical velocity cut-off be larger than the rms velocity $D_z(S)$ of turbulent field. The implication is clear: in the case $\nu \geq 2/3$ one cannot obtain the 'thin-slice' asymptote $R^{1-\nu/2}$. For $\nu < 2/3$, one might be able to see power-law behaviour $R^{1-\nu/2}$ before non-linear behaviour appears. On the other hand, at some intermediate scale R, absorption sets the width of the velocity kernel, and as explained in LP04 is of the order of $\Delta V \sim R^{\nu/2}$. In this situation, the scaling of the centroids is $R^{1-\nu/2}\Delta V \sim R$, and like in the VCA, centroids show an intermediate universal regime as well. In this regime, centroids lose information on the spectral slope of the velocity field. If one considers even smaller scale, then one should be able to recover the usual centroid scaling. In fact, if the velocity cut-off v_{ab} introduced by self-absorption is much larger the velocity dispersion of the turbulent field, one should be able to recover the usual centroid scaling $R^{1+\nu}$. In the subsonic regime, where $D_z(R) \ll \beta_T$, one should again be able to recover the usual centroid scaling. This is one of the major advantage of centroids over VCA, which loses information about velocity spectrum at subsonic scales. These scalings are summarized in Table 2, and part of the asymptotes are shown in Fig. 2.

In the absence of absorption, centroids are obtained by integrating over the entire LOS velocity, and therefore for a constant density field, the asymptote of centroid structure function scales as $\mathcal{D}(R) \sim R^{1+\nu}$. In the presence of absorption, although one should formally integrate over the entire LOS velocity, the integration range is effectively set by the extent of absorption. In this case, depending on the extent of absorption one may or may not be able to obtain the same scaling as in the absence of absorption. In fact, as shown

Table 2. Scaling of centroid structure function arising from pure velocity effects in the presence of absorption. The scaling $R^{1-\nu/2}$ is only present for $\nu < 2/3$. The corresponding scaling in the case of VCA is also presented for comparison.

Scale range	Centroid scaling	VCA scaling (integrated lines)	Regime
$R/S < \left(\frac{\beta_T}{D_z(S)}\right)^{1/\nu}$	$\mathcal{D}(R) \propto R^{1+\nu}$	Velocity effects erased	Subsonic
$R/S \ll \left(\frac{v_{ab}^2}{D_z(S)+2\beta_T}\right)^{1/\nu}$	$\mathcal{D}(R) \propto R^{1+\nu}$	$\mathcal{D}(R) \propto R^{1+\nu/2a}$	Thick slice
$R/S < \left(\frac{v_{ab}^2}{D_z(S)+2\beta_T}\right)^{1/\nu}$	$\mathcal{D}(R) \propto R$	$\mathcal{D}(R) \propto R$	Intermediate
$\left(\frac{v_{ab}^2}{D_z(S)+2\beta_T}\right)^{1/\nu} < R/S < \left(\frac{v_{ab}^2}{D_z(S)+2\beta_T}\right)^{2/(2-\nu)}$	$\mathcal{D}(R) \propto R^{1-\nu/2}$	$\mathcal{D}(R) \propto R^{1-\nu/2}$	Effectively[b] thin slice
$R/S > \left(\frac{v_{ab}^2}{D_z(S)+2\beta_T}\right)^{2/(2-\nu)}$	Not a power law	Not a power law	Strong absorption

Notes. [a]One will see saturation R^2 of the structure function after this scaling.
[b]The discussion on VCA involves integrated lines, and thus slice thickness is not set by interferometers but 'effectively' by the level of self-absorption.

in Fig. 2 and as summarized in Table 2, the asymptote might show different scaling at different lags R.

The most important finding is that in the presence of absorption, 'usual' centroids may not be recovered at all. In fact, as shown in Table 2, one might be able to see the usual scaling of $R^{1+\nu}$ only in a very restricted range of scales. Another important finding is that for sufficiently hot turbulent plasma, the centroids work well even when self-absorption is strong. This can be understood in the following way: if thermal effects are strong, then the effect of self-absorption is diminished. This is because for high temperature ρ_s becomes small, and therefore the intensity obtained from equation (2) looks more like that for an optically thin case. Our result that centroids work well for high temperatures even in the presence of self-absorption is a very distinct and useful result in comparison to VCA, which works well for recovering velocity statistics only when the velocity dispersion is larger than the thermal broadening.

4 CENTROIDS FOR ABSORPTION LINES

In the previous section (and also in the past works), emission lines were used to obtain centroids. However, if the turbulence cloud is between an observer and an extended emission source, one can also measure VCs for absorption lines. The turbulent motions affect the line profile, and thus one should be able to study turbulence using absorption lines. An advantage of studying turbulence with absorption lines is that multiple lines with various optical depths can be used simultaneously (KLP). Moreover, centroids are not sensitive to the gradients of wings of line profile, as multiplication by v (which is odd) to even gradients in left and right wings, and upon integration washes away the effect of these gradients. In the context of VCS, absorption lines were studied in LP08. It was shown that even in the presence of strong absorption line, one can obtain information on the turbulent spectra if one uses logarithm of intensity (i.e. optical depth) instead of intensity, and studies turbulence using the wings of the absorption line. The connection between the study carried out in LP08 and centroids is simple: instead of using centroids for intensity, one needs to use optical depth to define centroids. However, because centroids are obtained by integrating over entire spectral line, in contrast to LP08, we focus on spatial correlations between LOSs.

The profile of an absorption line is given by

$$I(\boldsymbol{X}) = I_0 \mathrm{e}^{-\tau(\boldsymbol{X}, v_1)}, \tag{28}$$

where $\tau(\boldsymbol{X}, v_1)$ is the optical depth. If intrinsic line broadening is ignored (see LP08 for details), the optical depth is given by

$$\tau(\boldsymbol{X}, v_1) = \alpha(v_0) \int_0^S \mathrm{d}z\, \rho(\boldsymbol{X}, z) \Phi(v_1 - u(z)), \tag{29}$$

The VC weighted by the optical depth can be defined as

$$C(\boldsymbol{X}) = \int \mathrm{d}v_1\, v_1 \log\left(\frac{I(\boldsymbol{X}, v_1)}{I_0}\right) = \int \mathrm{d}v_1\, v_1 \tau(\boldsymbol{X}, v_1). \tag{30}$$

Note that to obtain centroids, we used logarithm of intensity. Useful property of the centroids is that one does not need to precisely know the base-level I_0, since $v_1 \log I_0$ is an odd function, and vanishes upon performing the integration over v_1.

If one has information on the optical depth throughout the whole line, it is clear from equation (30) that by using logarithm of intensity of an absorption line, one can obtain the centroid structure function of the same form as that of optically thin emission lines (cf. equation 11), and thus one can obtain the same information about turbulence statistics.

However, real world observations have noise associated with them and therefore, realistically the profile of an absorption line is given by

$$I(\boldsymbol{X}) = I_0 \mathrm{e}^{-\tau(\boldsymbol{X}, v_1)} + N, \tag{31}$$

where N is the noise. Clearly for optical depths $\tau > -\log(N/I_0)$, the central part of the line is saturated below the noise level and the useful information is restricted to the wings of the line, where $\tau < -\log(N/I_0)$. For such case, we suggest to construct restricted centroids by integrating $\int \mathrm{d}v_1\, v_1 \tau(\boldsymbol{X}, v_1)$ just over the wings of the line, where optical depths can be accurately determined. To maintain the properties of centroids, one should integrate over a symmetric pair of intervals of width Δ centred at v_0 and $-v_0$ for the left and right wing (line is assumed to be centred at $v = 0$).

As an illustration, let us consider wings of the line to be selected by a sharp window. In this case, the restricted centroids are given by

$$C(\boldsymbol{X}) = \int_{-v_0-\Delta/2}^{-v_0+\Delta/2} \mathrm{d}v_1\, v_1 \tau(\boldsymbol{X}, v_1) + \int_{v_0-\Delta/2}^{v_0+\Delta/2} \mathrm{d}v_1\, v_1 \tau(\boldsymbol{X}, v_1), \tag{32}$$

where the centre of the wing v_0 is of the order of $\sqrt{D_z(S) + 2\beta_T}$. Formally, when Δ approaches $2v_0$ two wings overlap and the whole line is available for analysis.

Using the usual approach (see equations 8 and 13), one obtains the centroid correlation as

$$\xi(\boldsymbol{R}) = 2\left[\xi_{11}(\boldsymbol{R}) + \xi_{12}(\boldsymbol{R})\right], \tag{33}$$

where $\xi_{11}(\boldsymbol{R})$ denotes correlations within the same wing, and is given by

$$\xi_{11}(\boldsymbol{R}) \propto \int_{-S}^{S} \mathrm{d}z \int_{v_0-\Delta/2}^{v_0+\Delta/2} \mathrm{d}v_1\, v_1 \int_{v_0-\Delta/2}^{v_0+\Delta/2} \mathrm{d}v_2\, v_2 \times \frac{\xi_\rho(\boldsymbol{r})}{\sqrt{D_z(\boldsymbol{r})+2\beta_\mathrm{T}}} \exp\left[-\frac{(v_1-v_2)^2}{2(D_z(\boldsymbol{r})+2\beta_\mathrm{T})}\right] \sqrt{\frac{2}{D^+(S,\boldsymbol{r})}} \times \exp\left[-\frac{(v_1+v_2)^2}{4D^+(S,\boldsymbol{r})}\right], \tag{34}$$

and $\xi_{12}(\boldsymbol{R})$ denotes correlation between two wings, and is given by

$$\xi_{12}(\boldsymbol{R}) \propto \int_{-S}^{S} \mathrm{d}z \int_{v_0-\Delta/2}^{v_0+\Delta/2} \mathrm{d}v_1\, v_1 \int_{-v_0-\Delta/2}^{-v_0+\Delta/2} \mathrm{d}v_2\, v_2 \ldots, \tag{35}$$

where ... denotes that the integrand in equation (35) is the same as that in equation (34), but the integration range over v_1 and v_2 are non-overlapping.

We now investigate two extreme limits: first, $\Delta \to 0$. In this case, the integration over a narrow range of Δ can be approximated by evaluating the integrand at central value of the integration range. Thus, we have

$$\xi_{11}(\boldsymbol{R}) \propto \Delta^2 \int_{-S}^{S} \mathrm{d}z\, v_0^2 \frac{\xi_\rho(\boldsymbol{r})}{\sqrt{D_z(\boldsymbol{r})+2\beta_\mathrm{T}}} \sqrt{\frac{2}{D^+(S,\boldsymbol{r})}} \times \exp\left[-\frac{v_0^2}{4D^+(S,\boldsymbol{r})}\right], \tag{36}$$

and

$$\xi_{12}(\boldsymbol{R}) \propto -\Delta^2 \int_{-S}^{S} \mathrm{d}z\, v_0^2 \frac{\xi_\rho(\boldsymbol{r})}{\sqrt{D_z(\boldsymbol{r})+2\beta_\mathrm{T}}} \sqrt{\frac{2}{D^+(S,\boldsymbol{r})}} \times \exp\left[-\frac{2v_0^2}{(D_z(\boldsymbol{r})+2\beta_\mathrm{T})}\right]. \tag{37}$$

Since $v_0^2 \sim D^+(S,\boldsymbol{r})$, it is clear that due to an exponential suppression $\xi_{12}(\boldsymbol{R}) \ll \xi_{11}(\boldsymbol{R})$, and therefore for $\Delta \sim 0$ the correlation is given by

$$\xi(\boldsymbol{R}) \approx 2\xi_{11}(\boldsymbol{R}) \propto \Delta^2 \int_{-S}^{S} \mathrm{d}z\, v_0^2 \frac{\xi_\rho(\boldsymbol{r})}{\sqrt{D_z(\boldsymbol{r})+2\beta_\mathrm{T}}}. \tag{38}$$

At small scales, the factor $D^+(\boldsymbol{r})$ is close to constant, and therefore the asymptote in equation (38) fully depends on the form of the integrand $\xi_\rho(\boldsymbol{r})/\sqrt{D_z(\boldsymbol{r})+2\beta_\mathrm{T}}$. Looking at equation (38), one can see that for $D_z(\boldsymbol{R}) > 2\beta_\mathrm{T}$, one obtains an asymptote $R^{1-\nu/2}$ in the case of constant density field. This formally corresponds to the 'thin-slice' regime in the context of VCA. Indeed, as Δ and β_T become smaller, the integration channel slice becomes thinner, and this corresponds to returning to the thin-slice regime of VCA. In the case when Δ is finite, $D_z(\boldsymbol{R}) > 2(\beta_\mathrm{T}+\Delta^2)$ needs to be satisfied in order to achieve thin-slice asymptote.

The second case of interest is $\Delta = 2v_0$, which formally corresponds to two wings touching each other, which selects central section of the line of width 2Δ. Using equation (32), it can be shown that

$$\xi(\boldsymbol{R}) \propto \int_{-S}^{S} \mathrm{d}z \int_{-\Delta}^{\Delta} \mathrm{d}v_1\, v_1 \int_{-\Delta}^{\Delta} \mathrm{d}v_2\, v_2 \frac{\xi_\rho(\boldsymbol{r})}{\sqrt{D_z(\boldsymbol{r})+2\beta_\mathrm{T}}} \times \exp\left[-\frac{(v_1-v_2)^2}{2(D_z(\boldsymbol{r})+2\beta_\mathrm{T})}\right] \sqrt{\frac{2}{D^+(S,\boldsymbol{r})}} \exp\left[-\frac{(v_1+v_2)^2}{4D^+(S,\boldsymbol{r})}\right]. \tag{39}$$

It is easy to see from equation (39) that when $\Delta \to \infty$, the usual centroids are recovered. A less stringent criterion to recover centroids when $\Delta \sim \sqrt{D_z(S)+2\beta_\mathrm{T}}$ is to study turbulence at small lags R satisfying $D_z(R) < 2(\Delta^2+\beta_\mathrm{T})$. This condition can be achieved either for sufficiently short scales or for sufficiently large Δ and β_T. Physically, large Δ means entire line is available for centroids statistics, and it is natural to expect to recover usual centroids in such limit. Numerical integration confirms this, and this has been clearly shown in Fig. 3 and Table 3, where it is shown that at small scales R, the velocity spectrum is correctly given by the centroids. Note that with the thermal effects included, there is a larger range of lag R, which yields the usual centroid correlation.

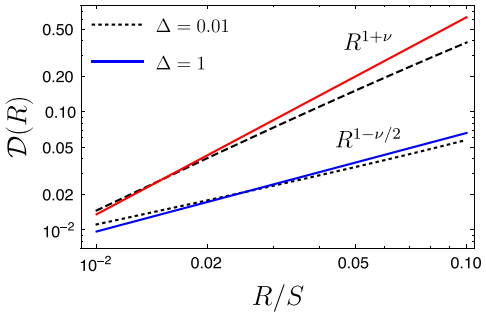

Figure 3. Centroid structure for broadening parameter $\Delta = 0.01$ and 1, and for a constant density field. For small Δ, the asymptote $R^{1-\nu/2}$ is reached fast, while for large Δ the asymptote $R^{1+\nu}$ is extended over large range of R. The effect of increasing temperature is effectively the same as increasing Δ. Example curves are produced for velocity field with Kolmogorov index $\nu = 2/3$.

Table 3. Scaling of centroid structure function arising from pure velocity effects in absorption line study.

Scale range	Centroid scaling
$R/S \lesssim \left(\frac{2(\Delta^2+\beta_\mathrm{T})}{D_z(S)}\right)^{1/\nu}$	$\mathcal{D}(R) \propto R^{1+\nu}$
$R/S \gtrsim \left(\frac{2(\Delta^2+\beta_\mathrm{T})}{D_z(S)}\right)^{1/\nu}$	$\mathcal{D}(R) \propto R^{1-\nu/2}$

5 CENTROID ANISOTROPY: GENERAL FORMALISM

In this section, the study of centroids will be carried out keeping in mind that the ISM is magnetized and therefore there exists a preferred direction, which in the global frame of reference is the direction of the mean magnetic field. Due to the presence of this preferred direction, turbulence is anisotropic; to be more precise, axisymmetric. This anisotropy is built in the general tensors representing velocity, density and magnetic field correlations. The study of magnetic correlation was carried out in LP12, and the study of velocity correlation and its application to study intensity anisotropies was carried out in KLP. In this paper, we present another way of

studying anisotropies, which is through the study of anisotropy of centroids correlation. The main focus of this section is to develop a general formalism to study centroid anisotropy in the presence of *constant* density field.

The Fourier component of a velocity field is in general given by $\boldsymbol{v}(\boldsymbol{k}) = a_k \hat{\xi}(\hat{\boldsymbol{k}}, \hat{\lambda})$, where $\boldsymbol{k}$ is the wavevector, a_k is the random amplitude of a mode (which in general has both real and imaginary parts) and $\hat{\xi}$ is the direction of allowed displacement in a plasma. With this definition, the velocity correlation in Fourier space is given by

$$\begin{aligned}\langle v_i(\boldsymbol{k}) v_j^*(\boldsymbol{k}')\rangle &= \langle a_k a_{k'}^*\rangle \left(\hat{\xi}_k \otimes \hat{\xi}_{k'}^*\right)_{ij} \\ &\equiv \mathcal{A}(k, \hat{\boldsymbol{k}}\cdot\hat{\lambda}) \left(\hat{\xi}_k \otimes \hat{\xi}_k^*\right)_{ij} \delta(\boldsymbol{k}-\boldsymbol{k}'),\end{aligned} \tag{40}$$

where $\mathcal{A}(k, \hat{\boldsymbol{k}}\cdot\hat{\lambda}) = \langle \hat{a}_k \hat{a}_k^*\rangle$ is the power spectrum, which for anisotropic turbulence depends on the angle $\mu_k \equiv \hat{\boldsymbol{k}}\cdot\hat{\lambda}$. To obtain velocity correlation tensor in the real space, one needs to carry out Fourier transform of equation (40)

$$\left\langle v_i(\boldsymbol{x}_1) v_j(\boldsymbol{x}_1+\boldsymbol{r})\right\rangle = \frac{1}{(2\pi)^3}\int \mathrm{d}^3\boldsymbol{k}\, \mathrm{e}^{\mathrm{i}\boldsymbol{k}\cdot\boldsymbol{r}} \mathcal{A}(k, \hat{\boldsymbol{k}}\cdot\hat{\lambda}) \left(\hat{\xi}_k \otimes \hat{\xi}_k^*\right)_{ij}. \tag{41}$$

The centroid structure function in the case of constant density for an optically thin medium is given by (cf. equation 15)

$$\mathcal{D}(R) \propto \int \mathrm{d}z (D_z(R,z) - D_z(0,z)). \tag{42}$$

In order to evaluate the above integral, we need to evaluate integral of the type $\int \mathrm{d}z \langle v_i v_j\rangle$. This can effectively be obtained by noting that the integration over the entire LOS is equivalent to setting $k_z = 0$ in the spectral domain (LP12). Therefore, we can write

$$\int \mathrm{d}z \langle v_i v_j\rangle = \frac{1}{(2\pi)^2}\int \mathrm{d}^2\boldsymbol{K}\, \mathrm{e}^{\mathrm{i}\boldsymbol{K}\cdot\boldsymbol{R}} \mathcal{A}(K, \hat{\boldsymbol{K}}\cdot\hat{\Lambda}) \left(\hat{\xi}_K \otimes \hat{\xi}_K^*\right)_{ij}. \tag{43}$$

We use the plane wave expansion

$$\mathrm{e}^{\mathrm{i}\boldsymbol{K}\cdot\boldsymbol{R}} = \mathrm{e}^{\mathrm{i}KR\cos\zeta_R} = \sum_{n=-\infty}^{\infty} \mathrm{i}^n J_n(KR) \mathrm{e}^{\mathrm{i}n\zeta_R}, \tag{44}$$

where $\cos\zeta_R = \hat{\boldsymbol{K}}\cdot\hat{\boldsymbol{R}}$. Similarly, decomposing the two-dimensional power spectra into series of harmonics

$$\mathcal{A}(K, \hat{\boldsymbol{K}}\cdot\hat{\Lambda}) = \sum_{p=-\infty}^{\infty} K^{-3-\nu} \hat{\mathcal{A}}_p \mathrm{e}^{\mathrm{i}p\zeta_\Lambda}, \tag{45}$$

where $\cos\zeta_\Lambda = \hat{\boldsymbol{K}}\cdot\hat{\boldsymbol{\Lambda}}$, we obtain

$$\begin{aligned}\int \mathrm{d}z \langle v_i v_j\rangle = \frac{1}{(2\pi)^2}\int \mathrm{d}\boldsymbol{K}\, K^{-2-\nu} \sum_{n=-\infty}^{\infty} \mathrm{i}^n \mathrm{e}^{\mathrm{i}n\phi} J_n(KR) \\ \times \sum_{p=-\infty}^{\infty} \hat{\mathcal{A}}_p \mathrm{e}^{-\mathrm{i}(n-p)\psi} \left(\hat{\xi}_K \otimes \hat{\xi}_K^*\right)_{ij},\end{aligned} \tag{46}$$

where $\cos\psi = \hat{\boldsymbol{K}}\cdot\hat{\boldsymbol{\Lambda}}$. Due to the axisymmetric nature of the turbulence, only even p is allowed in equation (45). With this, we finally obtain the following form of centroid structure function

$$\begin{aligned}\mathcal{D}(\boldsymbol{R}) = \frac{1}{(2\pi)^2}\int \mathrm{d}\boldsymbol{K}\, K^{-2-\nu} \sum_{n=-\infty}^{\infty} \mathrm{i}^n \mathrm{e}^{\mathrm{i}n\phi} (J_n(0)\delta_{n0} \\ - J_n(KR)) \sum_{p=-\infty}^{\infty} \hat{\mathcal{A}}_p \mathrm{e}^{-\mathrm{i}(n-p)\psi} \left(\hat{\xi}_K \otimes \hat{\xi}_K^*\right)_{zz},\end{aligned} \tag{47}$$

where n is even due to the fact that p is even. To study anisotropy of the structure function, it is convenient to expand the structure function in series of two-dimensional circular harmonics

$$\mathcal{D}(R,\phi) = \sum_{n=-\infty}^{\infty} \mathcal{D}_n(R) \mathrm{e}^{\mathrm{i}n\phi}, \tag{48}$$

where $\mathcal{D}_n(R)$ is the multipole moment of the centroid structure function given by (cf. equation 47)

$$\mathcal{D}_n(R) = C_n(\nu) \sum_{p=-\infty}^{\infty} \hat{\mathcal{A}}_p \mathcal{W}_{n-p} R^{1+\nu}, \tag{49}$$

and $\mathcal{W}_p$ is the spectral weight function, which is the integral of the tensor structure of a specific mode over the two-dimensional angle ψ, given by

$$\mathcal{W}_p = \frac{1}{2\pi}\int_0^{2\pi} \mathrm{d}\psi\, \mathrm{e}^{-\mathrm{i}p\psi} \left(\hat{\xi}_K \otimes \hat{\xi}_K^*\right)_{zz}, \tag{50}$$

and

$$\begin{aligned}C_n(\nu) &= \mathrm{i}^n \int \mathrm{d}K\, K^{-2-\nu} (J_n(0)\delta_{n0} - J_n(K)) \\ &= -\frac{\mathrm{i}^n \Gamma\left[\frac{1}{2}(|n| - \nu - 1)\right]}{2^{2+\nu}\Gamma\left[\frac{1}{2}(|n| + \nu + 3)\right]}.\end{aligned} \tag{51}$$

Equations (48) and (49) are the main equations that will be used subsequently to obtain centroid structure function of each MHD modes. A useful parameter for comparison with past numerical work is the isotropy degree, defined as

$$\text{Isotropy degree} = \frac{\mathcal{D}(R, \phi = 0)}{\mathcal{D}(R, \phi = \pi/2)}. \tag{52}$$

6 CENTROIDS FOR DIFFERENT MHD MODES

The properties of MHD turbulence depends on the degree of magnetization. The Alfvén Mach number $M_\mathrm{A} = V_L/V_\mathrm{A}$, where V_L is the injection velocity at the scale L and V_A is the Alfvén velocity, presents a useful measure of magnetization. Depending on whether $M_\mathrm{A} > 1$, $M_\mathrm{A} = 1$ or $M_\mathrm{A} < 1$, turbulence can be super-Alfvénic, trans-Alfvénic or sub-Alfvénic. For $M_\mathrm{A} \gg 1$, magnetic forces are not important at large scales and the cascade should be similar to ordinary hydrodynamic cascade in the vicinity of the injection scale. The seminal paper by Goldreich & Sridhar (1995, hereafter GS95) ushered the modern understanding of MHD turbulence. The GS95 was formulated for trans-Alfvénic turbulence, and the generalization of GS95 for sub-Alfvénic and super-Alfvénic cases can be found in Lazarian & Vishniac (1999). The original GS95 theory was elaborated in further studies, in particular, the concept of local system of reference (Lazarian & Vishniac 1999; Cho & Vishniac 2000; Maron & Goldreich 2001; Cho, Lazarian & Vishniac 2002) was introduced. According to this concept, turbulent motions should not be viewed in the system of reference of the mean magnetic field as all earlier theories of MHD turbulence attempted to do, but in the system of reference of magnetic field comparable with the size of the eddies. However, from the point of view of the observational studies of the turbulence in a volume when the only available statistics are those averaged along the LOS, the measurements should be carried out in the system of mean magnetic field, rather than the local system of reference. Therefore, one has to describe Alfvénic turbulence in the global system of reference (see the discussions in Cho & Lazarian 2002; Esquivel & Lazarian 2005, LP12). This modifies the available statistics. For instance, in the local system of

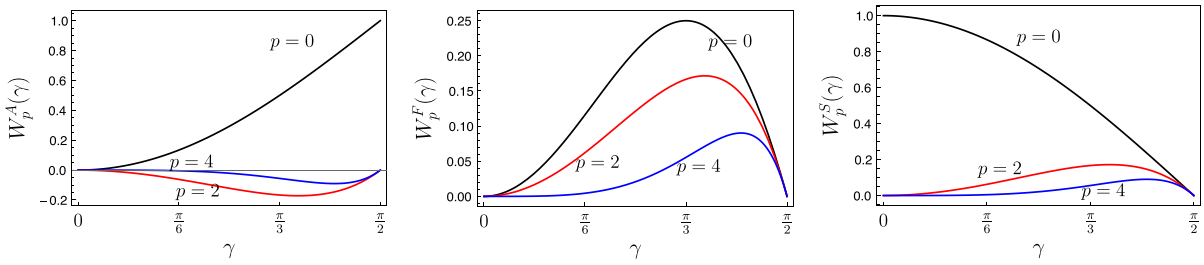

Figure 4. From left to right: spectral function of Alfvén mode $W_p^A(\gamma)$ (left-hand panel), low-β fast mode $W_p^F(\gamma)$ (centre) and high-β slow mode $W_p^S(\gamma)$ (right-hand panel) for various index p (which is $n-p$ in equation 49).

reference GS95 predict the existence of two different energy spectra, namely, the parallel and perpendicular, in the global system of reference only the spectrum of dominant perpendicular fluctuations is available. Similarly, while in the local system of reference the anisotropy increases with the decrease of size of the eddies, the anisotropy stays constant in the global system of reference.

MHD turbulence can be presented as a superposition of interacting fundamental modes, i.e. Alfvén, slow and fast. The first theoretical considerations in favour of this were given in GS95 (see also Lithwick & Goldreich 2001), which were extended and numerically tested in Cho & Lazarian (2002, 2003) and in Kowal & Lazarian (2010). Because the compressible and incompressible modes weakly exchange their energy[2] (Cho & Lazarian 2002), it is possible to consider the modes separately.

With this background discussion of MHD turbulence, we are ready to proceed to study centroids anisotropy in detail. In this section, we will employ our previous expression to obtain centroids for different MHD modes. We will use the tensor structures obtained by KLP for our discussion. These expressions will be used in the next section to specific MHD mode in order to study anisotropy due to each MHD mode.

6.1 Alfvén mode

Alfvén modes are incompressible, and their tensor should also reflect this. The correlation function of Alfvén mode is obtained by employing the condition that the displacement of this mode in a plasma is orthogonal to the wavevector and the direction of magnetic field, and is given by (see KLP)

$$\left(\hat{\xi}_{\boldsymbol{k}} \otimes \hat{\xi}^*_{\boldsymbol{k}}\right)_{ij} = \left(\delta_{ij} - \hat{k}_i \hat{k}_j\right) - \frac{(\hat{\boldsymbol{k}}\cdot\hat{\lambda})^2 \hat{k}_i \hat{k}_j + \hat{\lambda}_i \hat{\lambda}_j - (\hat{k}\cdot\hat{\lambda})(\hat{k}_i\hat{\lambda}_j + \hat{k}_j\hat{\lambda}_i)}{1-(\hat{\boldsymbol{k}}\cdot\hat{\lambda})^2}. \tag{53}$$

In LP12, the first part of the above tensor was referred to as 'E-type', while the second part was referred to as 'F-type'. Both E and F-type parts are divergence free, and therefore the velocity field in Alfvén modes is purely solenoidal. For an isotropic power spectra $\mathcal{A}$, the E-part yields isotropic correlation tensor, while F-part still gives rise to anisotropy. Making use of equation (53), we obtain

$$\left(\hat{\xi}_K \otimes \hat{\xi}^*_K\right)_{zz} = 1 - \frac{\hat{\lambda}_z\hat{\lambda}_z}{1-(\hat{\boldsymbol{K}}\cdot\hat{\Lambda})^2} = \sin^2\gamma\,\frac{\sin^2\psi}{1-\sin^2\gamma\cos^2\psi}, \tag{54}$$

[2] This was recently shown to be also true for relativistic MHD turbulence in Takamoto & Lazarian (2016).

where $\cos\gamma = \hat{r}\cdot\hat{\lambda}$, and $0 \le \gamma \le \pi/2$. Note that correlation given by equation (54) vanishes at $\gamma = 0$, which is expected as motions are perpendicular to the magnetic field. Making use of equations (49) and (54), the multipole moments of centroid structure function for Alfvén mode can be written as

$$\mathcal{D}_n(R) = C_n(2/3)\sum_{p=-\infty}^{\infty} \hat{\mathcal{A}}_p \mathcal{W}^A_{n-p} R^{5/3}, \tag{55}$$

where $\hat{\mathcal{A}}_p$ is the coefficient of two-dimensional harmonic expansion of power spectrum, and, as suggested in (Cho & Lazarian 2002), is given by

$$\hat{\mathcal{A}}_p = \frac{1}{2\pi}\int_0^{2\pi} \mathrm{d}\psi\, \mathrm{e}^{-\mathrm{i}p\psi} \exp\left[-M_{\rm A}^{-4/3}\frac{|\cos\psi|\sin\gamma}{(1-\cos^2\psi\sin^2\gamma)^{2/3}}\right], \tag{56}$$

and $\mathcal{W}^A_{n-p}$ spectral weight defined as

$$\mathcal{W}^A_{n-p} = \frac{1}{2\pi}\int_0^{2\pi} \mathrm{d}\psi\, \mathrm{e}^{-\mathrm{i}(n-p)\psi}\frac{\sin^2\gamma\sin^2\psi}{1-\sin^2\gamma\cos^2\psi}. \tag{57}$$

An analytical form of this spectral weight exists and is given by

$$\mathcal{W}^A_{n-p} = \delta_{p,n} - \cos\gamma\left(\frac{1-\cos\gamma}{\sin\gamma}\right)^{|n-p|}. \tag{58}$$

It is clear from equations (55) and (57) that the centroid structure function of Alfvén mode vanishes at $\gamma = 0$, which reflects that there is no LOS component of the Alfvén velocity when magnetic field is along the LOS. In the opposite case $\gamma = \pi/2$ when magnetic field is perpendicular to the LOS, $\mathcal{W}^A_{n-p} = \delta_{pn}$, and multipole moments of the centroid structure function $\mathcal{D}_n(R) \propto \mathcal{A}_n$. It can be clearly seen from the left-hand panel of Fig. 4. For general γ, it is also clear from the figure that the magnitude of the function $\mathcal{W}^A_{n-p}$ decays rapidly as $|n-p|$ increases. This means that for our practical purposes, it is enough to just few terms near $p \approx n$ in the sum presented in equation (55).

Fig. 5 shows some important properties of Alfvén mode. First, looking at this figure one can clearly see that this mode becomes more isotropic with increasing Alfvén Mach number $M_{\rm A}$, as characterized by the decreasing level of quadrupole to monopole and octupole to monopole ratio and increasing level of isotropy degree with increasing $M_{\rm A}$. It is also quite clear from the left-hand and central panel of the figure that this mode becomes highly anisotropic at $\gamma = \pi/2$, which is expected. Note that the finite quadrupole to monopole ratio at $\gamma = 0$ is misleading in a sense that both quadrupole and monopole vanish at $\gamma = 0$. In the case when one considers the mixture of modes, this problem is remedied as slow modes and high-β fast modes have non-vanishing monopole at $\gamma = 0$.

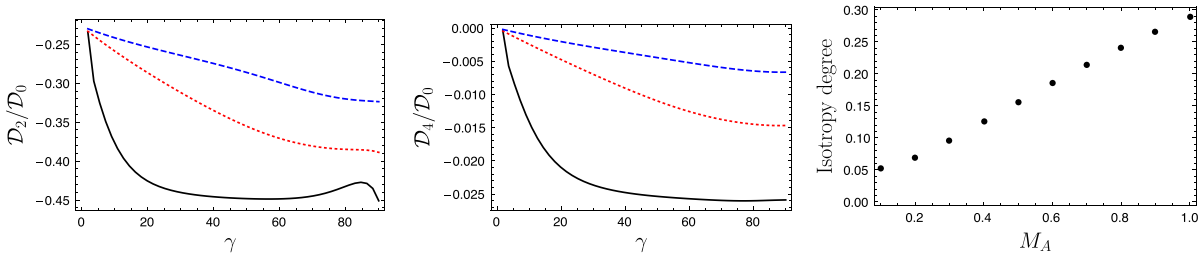

Figure 5. Alfvén mode. Left-hand panel and centre: quadrupole to monopole and octupole to monopole ratio for various γ. Solid line is for $M_{\rm A} = 0.1$, dotted line for $M_{\rm A} = 0.4$ and dashed line for $M_{\rm A} = 0.7$. Right-hand panel: isotropy degree for various $M_{\rm A}$ at $\gamma = \pi/2$.

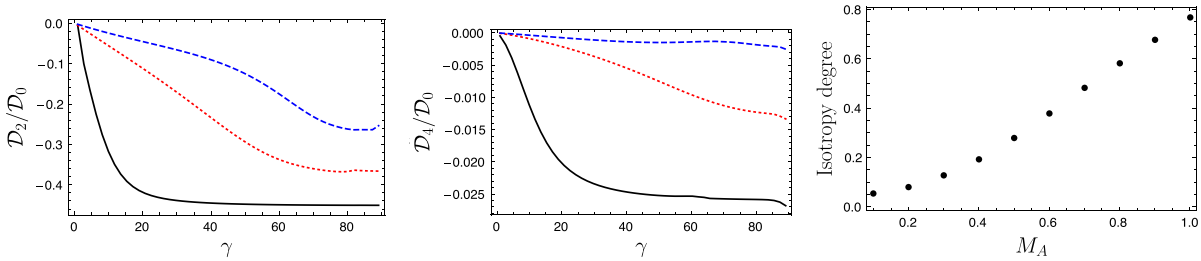

Figure 6. High-β slow mode. Left-hand panel and centre: quadrupole to monopole and octupole to monopole ratio for various γ. Solid line is for $M_{\rm A} = 0.1$, dotted line for $M_{\rm A} = 0.4$ and dashed line for $M_{\rm A} = 0.7$. Right-hand panel: isotropy degree for various $M_{\rm A}$ at $\gamma = \pi/3$.

6.2 Slow mode

Slow modes in high-β plasma are similar to pseudo-Alfvén modes in incompressible regime, while at low β they are density perturbations propagating with sonic speed parallel to magnetic field (see Cho & Lazarian 2003). The power spectrum of this mode is the same as that of Alfvén mode. Slow modes in high β are purely F-type and therefore, the correlation is given by (see KLP)

$$\left(\hat{\xi}_{\boldsymbol{k}} \otimes \hat{\xi}^*_{\boldsymbol{k}}\right)_{ij} = \frac{(\hat{\boldsymbol{k}}\cdot\hat{\lambda})^2\hat{k}_i\hat{k}_j + \hat{\lambda}_i\hat{\lambda}_j - (\hat{k}\cdot\hat{\lambda})\left(\hat{k}_i\hat{\lambda}_j + \hat{k}_j\hat{\lambda}_i\right)}{1 - \left(\hat{\boldsymbol{k}}\cdot\hat{\lambda}\right)^2}. \quad (59)$$

With this, we can write

$$\left(\hat{\xi}_{\boldsymbol{K}} \otimes \hat{\xi}^*_{\boldsymbol{K}}\right)_{zz} = \frac{\hat{\lambda}_z\hat{\lambda}_z}{1 - (\hat{\boldsymbol{K}}\cdot\hat{\Lambda})^2} = \frac{\cos^2\gamma}{1 - \sin^2\gamma\cos^2\psi}. \quad (60)$$

Using equations (49) and (60), one can obtain the multipole moments of the centroid structure function as

$$\mathcal{D}_n(R) = C_n(2/3)\sum_{p=-\infty}^{\infty}\hat{A}_p\mathcal{W}^S_{n-p}R^{5/3}, \quad (61)$$

where the spectral weight function $\mathcal{W}^S_p$ is given by

$$\mathcal{W}^S_{n-p} = \frac{1}{2\pi}\int_0^{2\pi} {\rm d}\psi\, {\rm e}^{-{\rm i}(n-p)\psi}\frac{\cos^2\gamma}{1-\cos^2\psi\sin^2\gamma} = \cos\gamma\left(\frac{1-\cos\gamma}{\sin\gamma}\right)^{|n-p|}. \quad (62)$$

The spectral weight function of slow modes, given by equation (62), is plotted in the left-hand panel of Fig. 4. It is clear from Fig. 4 that $\mathcal{W}^S_{n-p}$ vanishes at $\gamma = \pi/2$ for all $n-p$, and therefore the structure function vanishes at this angle. In the opposite case, $\gamma = 0$, $\mathcal{W}^S_{n-p}$ vanishes for all non-zero $n-p$ and equal to 1 for $n = p$, but $\hat{\mathcal{A}}_p = 0$ for $p > 0$; therefore, no anisotropy is present. For general γ, $\mathcal{W}^S_{n-p}$ decays very rapidly with increasing $|n-p|$, which implies that for practical purposes, it is enough up to just a few terms near $p \approx n$ in the sum presented in equation (61).

Slow modes in low β have their correlation function as $\langle v_i v_j\rangle \propto \hat{\lambda}_i\hat{\lambda}_j$ and therefore, it can be straightforwardly shown that

$$\mathcal{D}_n(R) = C_n(2/3)\cos^2\gamma\,\hat{\mathcal{A}}_n R^{5/3}. \quad (63)$$

Slow modes in both high- and low-β plasma are highly anisotropic at small $M_{\rm A}$ and become more isotropic with increasing $M_{\rm A}$. This is clearly shown in Figs 6 and 7. Moreover, the anisotropy level of both high- and low-β slow modes are similar. This is because the dominant term in equation (61) is the diagonal term $n = p$, while the $\cos^2\gamma$ term in equation (63) cancels upon taking ratio of multipole moments, thus the ratio of multipole moments in both cases yield similar results. It is important to note that the anisotropy of slow modes at $\gamma = \pi/2$ cannot be measured as both quadrupole and monopole vanish at $\gamma = \pi/2$.

6.3 Fast mode

Fast modes in high β are purely compressible modes with a velocity tensor structure given by

$$\left(\hat{\xi}_{\boldsymbol{k}} \otimes \hat{\xi}^*_{\boldsymbol{k}}\right)_{ij} = \hat{k}_i\hat{k}_j. \quad (64)$$

The power spectrum of fast modes is isotropic, and therefore the velocity correlation tensor is isotropic as well.

On the other hand, low-β fast mode is anisotropic with the anisotropy built in the tensor (see KLP)

$$\left(\hat{\xi}_{\boldsymbol{k}} \otimes \hat{\xi}^*_{\boldsymbol{k}}\right)_{ij} = \frac{\hat{k}_i\hat{k}_j - (\hat{k}.\hat{\lambda})\left(\hat{k}_i\hat{\lambda}_j + \hat{k}_j\hat{\lambda}_i\right) + (\hat{k}.\hat{\lambda})^2\hat{\lambda}_i\hat{\lambda}_j}{1 - (\hat{k}.\hat{\lambda})^2}. \quad (65)$$

Making use of equation (65), we obtain

$$\left(\hat{\xi}_{\boldsymbol{K}} \otimes \hat{\xi}^*_{\boldsymbol{K}}\right)_{zz} = \frac{(\sin\gamma\cos\gamma)^2\cos^2\psi}{1 - \sin^2\gamma\cos^2\psi}. \quad (66)$$

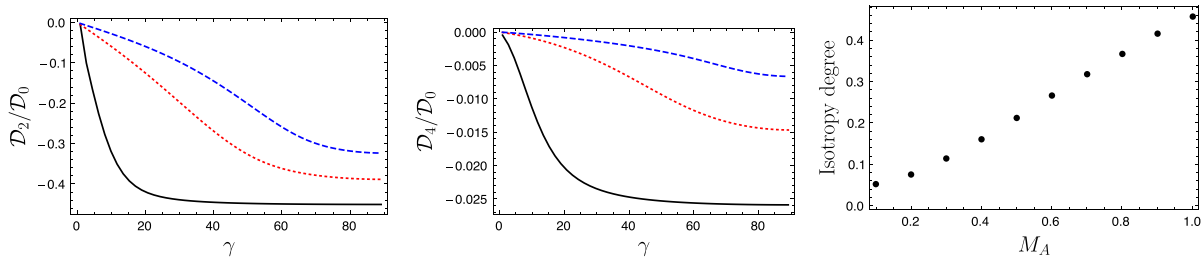

Figure 7. Low-β slow mode. Left-hand panel and centre: quadrupole to monopole and octupole to monopole ratio for various γ. Solid line is for $M_\mathrm{A} = 0.1$, dotted line for $M_\mathrm{A} = 0.4$ and dashed line for $M_\mathrm{A} = 0.7$. Right-hand panel: isotropy degree for various M_A at $\gamma = \pi/3$.

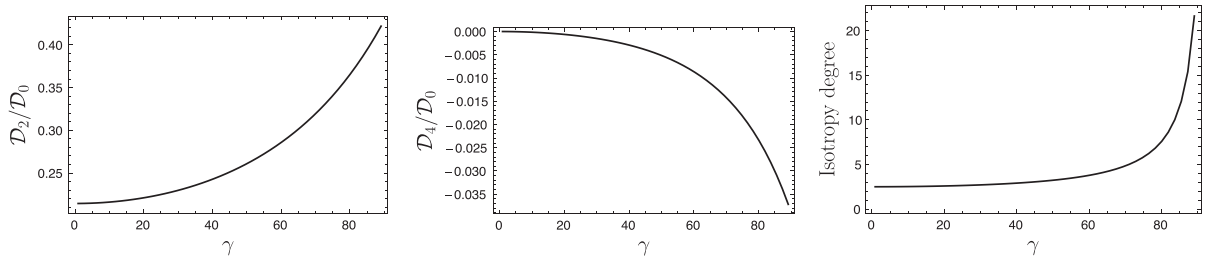

Figure 8. Low-β fast mode. Left-hand panel to right-hand panel: quadrupole to monopole, octupole to monopole ratio and isotropy degree for various γ.

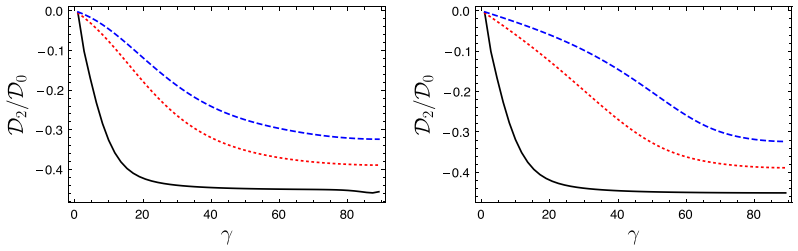

Figure 9. Mixture of modes. Left-hand panel: quadrupole to monopole ratio for a mixture of 85 per cent Alfvén and 15 per cent high-β slow modes. Right-hand panel: same for a mixture of 50 per cent Alfvén and 50 per cent low-β slow modes. Solid line is for $M_\mathrm{A} = 0.1$, dotted line for $M_\mathrm{A} = 0.4$ and dashed line for $M_\mathrm{A} = 0.7$.

Keeping in mind that fast modes have isotropic power spectrum so that only $\hat{\mathcal{A}}_0$ in non-vanishing, we have

$$\mathcal{D}_n(R) = C_n(1/2)\mathcal{A}_0\mathcal{W}_n^F R^{3/2}, \tag{67}$$

where the spectral weight function W_n^F is defined as

$$\mathcal{W}_n^F = \frac{1}{2\pi}\int_0^{2\pi} \mathrm{d}\psi\, \mathrm{e}^{-\mathrm{i}n\psi}\, \frac{(\sin\gamma\cos\gamma)^2\cos^2\psi}{1-\sin^2\gamma\cos^2\psi}$$
$$= -\cos^2\gamma\delta_{n0} + \cos\gamma\left(\frac{1-\cos\gamma}{\sin\gamma}\right)^{|n|}. \tag{68}$$

This spectral weight function of fast mode is plotted in the central panel of Fig. 4, which shows that this function vanishes both at $\gamma = 0$ and $\gamma = \pi/2$. The left-hand panel of Fig. 8 shows that the quadrupole to monopole ratio of low-β fast mode is $\sim$0.3 throughout the entire range of γ. The quadrupole to monopole ratio somewhat increases with increasing γ to its maximum value $\approx$0.4 at $\gamma = \pi/2$; however, the amplitude of both monopole and quadrupole is $\sim$0 at $\gamma \sim \pi/2$. In fact, the optimal signal is obtained at $\gamma \sim \pi/3$.

Note that since $C_2(1/2) > 0$, the quadrupole moment of fast mode is positive, which is also distinct from Alfvén mode. We found that this is due to the fact that anisotropy of fast mode comes from its anisotropic tensor structure and not from its power spectrum.

6.4 Mixture of modes

Real world setting of MHD turbulence involves superposition of the different MHD modes. Therefore, we consider the effect of mixtures of different MHD modes in the observed centroids anisotropy. In the case of mixture between Alfvén and slow modes, Fig. 9 clearly shows that the observed anisotropy is unaffected by this mixture in different regimes. For instance at $\gamma \gtrsim \pi/4$, the observed anisotropy of the mixture is the same as that of Alfvén mode alone while at $\gamma \lesssim \pi/4$, the anisotropy level is similar to that of slow modes alone. This is again due to the fact that at $\gamma \approx \pi/2$ signal from Alfvén mode is dominant, while at $\gamma \approx 0$ signal from slow mode is dominant. On the other hand, we expect the mixture of fast mode with other two modes to decrease the level of anisotropy. This is because the quadrupole moment (which is the measure of anisotropy) of fast mode is opposite in sign than that of other modes.

6.5 Density effects

The main aim of using VCs is to obtain information about velocity spectrum. Looking at equation (15), one can see that the centroid structure function contains not only the contribution from velocity effects but also from density effects. In this regard, separating velocity contribution from density contribution is not always possible. In particular, if the density spectrum is shallow, as is the case for

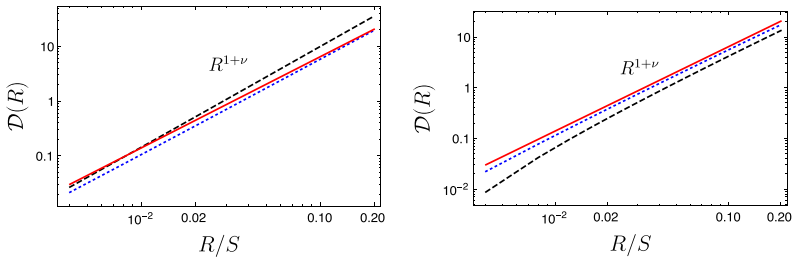

Figure 10. First panel: MVC structure function for various σ_ρ/ρ_0 for steep velocity field of Kolmogorov index 2/3 and density fields of index $\nu_\rho = 1/2$. The solid line is the expected power law of $R^{5/3}$, the dotted line is for $\sigma_\rho/\rho_0 = 0.5$ and the dashed line for $\sigma_\rho/\rho_0 = 1$. One can see some deviation from the power-law behaviour already at $\sigma_\rho/\rho_0 = 1$. This deviation is expected to be stronger with increasing σ_ρ/ρ_0. Second panel: the same but for shallow density with $\nu_\rho = -1/2$. The dotted line is for $\sigma_\rho/\rho_0 = 0.5$ and dashed line is for $\sigma_\rho/\rho_0 = 1$. Solid line is the power-law $R^{5/3}$ from pure velocity effects.

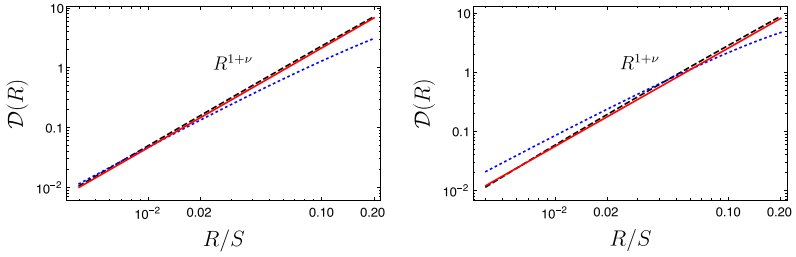

Figure 11. Plot showing comparison of MVC with UVC at $\sigma_\rho/\rho_0 = 0.5$ at short scales $R < S$. The dashed line in both the panels are for MVC, dotted line is for UVC and solid line shows the power-law $R^{5/3}$ from pure velocity effects. In both figures, a steep velocity spectrum of Kolmogorov index is assumed, whereas density spectrum is assumed to be steep (with $\nu_\rho = 1/2$) in the first panel and shallow (with $\nu_\rho = -1/2$) in the second. It is clear that MVC works well for both steep and shallow spectra.

supersonic turbulence, one might not be able to obtain the velocity spectra from the centroids. On the other hand, for a steep density spectra the velocity spectra can be extracted if the density dispersion in a turbulent field is less than the mean density (Esquivel et al. 2007). This has been clearly illustrated in the left-hand panel of the Fig. 10, where the centroid structure function is plotted for various ratios of σ_ρ/ρ_0. It is clearly shown in the figure that the velocity spectra can be obtained when $\sigma_\rho/\rho_0 < 1$, while the spectra are corrupted by the density–velocity cross-term when $\sigma_\rho/\rho_0 > 1$.

As explained in LE03, centroids can trace the velocity spectrum if the centroid structure function is much larger than the first term of equation (15). If this condition is not fulfilled, the velocity spectrum can be obtained by subtracting the first term (product of velocity dispersion and density correlation) of equation (15) as long as the density correlation can be measured independently[3] and density–velocity correlation is not strong. A potential challenge is the determination of velocity dispersion in the case when thermal broadening is large. However, one can circumvent this by using emission lines of heavier species. In this regard, LE03 introduced a notion of 'modified' velocity centroids (MVCs), where the first term of equation (15) was subtracted. Formally, the structure function of MVC in the absence of density–velocity correlation is

$$\mathcal{D}_{\rm MVC}(\boldsymbol{R}) \approx \int_{-S}^{S} {\rm d}z[\xi_\rho(\boldsymbol{r}) D_z(\boldsymbol{r}) - \xi_\rho(0,z) D_z(0,z)]. \quad (69)$$

It was explained in LE03 that MVCs can trace the velocity spectrum better than the UVCs if the lag R under study be smaller than the saturation scale of the velocity structure function as well as the LOS extent S of the turbulent cloud. We find that the MVC is able to trace the velocity spectra even for a shallow spectrum, as illustrated in Fig. 10. In fact, Fig. 11 clearly shows that modified centroids work better than UVC at smaller lags R. Note that for shallow density field, density–velocity cross-term yields a scaling $R^{1+\nu_\rho+\nu}$, while pure velocity term yields $R^{1+\nu}$, and since $\nu_\rho < 0$ for a shallow density spectra, this cross-term scaling can dominate the MVC scaling extremely small scale. Although, we see that MVCs work well even for shallow density spectra, there are two important points to make. First, we require $\sigma_\rho/\rho_0 < 1$ to obtain velocity spectra correctly, otherwise density–velocity correlation (which we ignored) becomes important (Esquivel et al. 2007). However, shallow density often does not fulfil this criterion. Secondly, shallow density is often associated with high sonic Mach number $M_{\rm s}$ where non-Gaussian features are often prominent, significantly affecting the statistics. To sum up, one needs to know if σ_ρ/ρ_0 to conclude if MVCs work for shallow spectra.

Our study of anisotropy was for constant density field. In the case when density field is anisotropic, one should also account for the anisotropy due to density effects as well. For MVC, the anisotropy is dominated by velocity effects as long as the density dispersion is less than the mean density. On the other hand, both density and velocity effects contribute to the UVC anisotropy.

6.6 Comparisons with earlier numerical works

The numerical study of anisotropies with centroids has been carried out in the past in LE03, Esquivel & Lazarian (2011, hereafter EL11) and Burkhart et al. (2014, hereafter BX14). Here, we compare our findings with the findings of EL11 and BX14. EL11 studied anisotropies at $\gamma = \pi/2$, while BX14 studied anisotropy at varying γ as well. Both of these studies found out a clear dependence of anisotropy with Alfvén Mach number $M_{\rm A}$. They reported that the

[3] Note that one can obtain this contribution from the density term observationally by measuring intensity fluctuations. For instance, in the language of VCA this term can be obtained through intensity statistics in the 'thick-slice' limit (see LP00 for more details).

anisotropy increases with decreasing M_A, which coincides with our result. As an example, at $M_A = 0.7$ and $M_s = 2.3$, the degree of isotropy in both the papers was reported to be ∼0.3, while our results show that in the case when Alfvén and slow modes are dominant, the isotropy degree at $M_A = 0.7$ is around ∼0.25, which is close to their results. Our finding that the degree of anisotropy is highest at $\gamma = \pi/2$ matches with the findings in BX14, where it was stated that at $\gamma = \pi/2$ the anisotropy is highest regardless of the sonic Mach number M_s. It is clear from our finding that the isotropy degree of centroid is clearly dependent on M_A. However, it was discussed in EL11 and BX14 that besides a dependence of isotropy degree of M_A, there exists a weak dependence on M_s as well. Although there is no direct role of M_s in determining the degree of isotropy in our formalism, this weak dependence can be explained by noting that with an increasing M_s, there is an increasing contribution from fast mode, thus decreasing the level of anisotropy. This is consistent with the results in EL11 and BX14.

6.7 Effects of self-absorption in anisotropy studies

In Sections 5 and 6, we studied anisotropy for an optically thin medium. With the theory developed in Section 3, it is straightforward to extend the study of anisotropy to optically thick media.

The extent of self-absorption sets an effective cut-off in velocity difference beyond which signals do not contribute to the correlation, and thus we may expect changes in anisotropy level as this extent changes. Our study in Section 3 suggests that in the case of weak self-absorption, the centroid structure function behaves similar to that of optically thin regime, while at stronger self-absorption it behaves as thin-slice regime of VCA (see LP00). Naturally, in this case of weak self-absorption one should see the level of anisotropy similar to the optically thin case of usual centroids, while at stronger self-absorption the anisotropy level will decrease to the level of thin-slice regime of VCA. For example, the isotropy degree of Alfvén mode at $M_A = 0.7$ and at $\gamma = \pi/2$ changes from 0.25 at weak absorption to 0.68 at strong absorption.

Interesting is the dependence of anisotropy level on the scale R. As shown in Table 2, in the presence of self-absorption structure function of centroids goes through different regimes as R changes. Thus, the anisotropy level is expected to behave differently at different lags R. In particular, at small R in thick-slice regime, the anisotropy level will be similar to the optically thin case of usual centroids, and this level will decrease with increase of R as one passes through the universal regime towards the thin-slice regime. This is demonstrated in Fig. 12. Thus, the isocorrelation contours

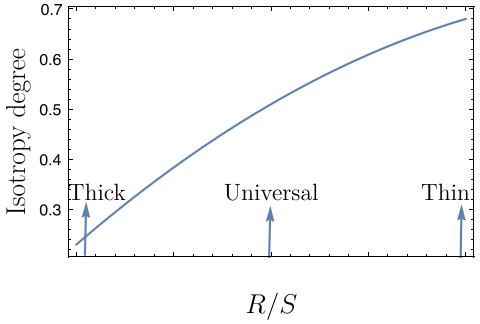

Figure 12. Expected change of isotropy degree at various scales R in the presence of self-absorption for Alfvén mode at $M_A = 0.7$ and at $\gamma = \pi/2$. The curve is produced by using three theoretically predicted values of isotropy degree at thick slice (usual centroids), universal regime and thin slice while intermediate values were obtained by interpolation.

are more elongated at small R and becomes more circular at large R.

Anisotropies in absorption line studies also show similar features. If absorption line is not saturated and the entire line is available for analysis, anisotropy level of centroid correlations will be similar to that of optically thin centroids. However, if absorption line is strong and only narrow portion of the wing is available for analysis, the anisotropy level will decrease reaching its minimum when the width of wing is essentially a delta function, and this minimum corresponds to the anisotropy level of thin-slice regime in VCA.

7 CENTROIDS AND INTERFEROMETRIC DATA

Interferometric output can be used to directly measure spectra and anisotropy of the UVC statistics using the Fourier spatial components of the intensity distribution that are available with interferometers. With interferometer, one can obtain spectral intensity and multiply this with the LOS velocity, and integrate this product over the entire frequency range to obtain centroid information. The study of centroids in Fourier domain is carried out in Dutta (2016), where potential of centroids to recover the turbulent velocity spectrum from radio interferometric observations is studied numerically.

To study anisotropies using centroids, one can also use raw interferometric data. Anisotropic feature needs information of two-dimensional maps, and therefore it is important to sample the fluctuations from different directions of the two-dimensional $\boldsymbol{K}$ space. The turbulence anisotropy is manifested as the anisotropy of the power spectrum of interferometric data, and thus we write the power spectrum as

$$P(\boldsymbol{K}) = \sum_{n=-\infty}^{\infty} P_n(K) \mathrm{e}^{-\mathrm{i}n\phi_K}. \tag{70}$$

Let us determine what information the measured P_n coefficients can provide. Utilizing equations (48) and (70), one can clearly write

$$P_n(K) = \int \mathrm{d}^2\boldsymbol{R}\, \mathcal{D}_n(R) \mathrm{e}^{-\mathrm{i}\boldsymbol{K}\cdot\boldsymbol{R}}, \tag{71}$$

which upon carrying out the angular integral yields

$$P_n(K) = \int \mathrm{d}R\, R \mathcal{D}_n(R) J_n(KR), \tag{72}$$

where $J_n(KR)$ is the Bessel function of the first kind. In the case of $K \gg R^{-1}$, the multipole moment in Fourier space has an asymptotic form

$$P_n(K) = \mathcal{D}_n(\nu) \frac{2^{2+\nu}\Gamma\left(\frac{1}{2}(|n| - \nu + 3)\right)}{\Gamma\left(\frac{1}{2}(|n| + \nu - 1)\right)} (KS)^{3+\nu}, \tag{73}$$

where $\mathcal{D}_n(\nu)$ is the real space centroid structure moment after explicitly factoring out R dependence, which for a constant density field is given by (cf. equation 49)

$$\mathcal{D}_n(\nu) = C_n(\nu) \sum_{p=-\infty}^{\infty} \hat{\mathcal{A}}_p \mathcal{W}_{n-p}. \tag{74}$$

It is clear from equation (73) that the centroid multipole moment in real space has one to one correspondence with that in the Fourier space, and the ratio of multipole moments in Fourier space is the same as that in real space. Therefore, by obtaining centroid anisotropy in Fourier space through interferometric data, one should be able to construct what that anisotropy corresponds to in real space. It should be stressed that this technique can also be used to obtain spectra of the velocity field.

The study in Esquivel & Lazarian (2005) suggests that MVCs might better reflect velocity statistics than UVCs. Thus, we believe that interferometric studies might also benefit by using MVCs. Since MVCs are defined only through the centroid structure function, MVCs in interferometric studies are equivalently defined through modified power spectrum by subtracting the product of velocity dispersion and power spectrum of column-density fluctuations. An elaborate technique equivalent to MVC would be to use fitting procedure with a supplied power spectrum of density fluctuations at sufficiently large K to determine the velocity spectra. The advantage of the fitting procedure is one does not need to know the velocity dispersion.

8 MAJOR FINDINGS OF THIS PAPER

The focus of this paper is the description of unnormalized centroids for turbulence studies. The novel part of the paper is the description of the marked effects of absorption on the unnormalized centroids, and the description of centroid anisotropy based on the decomposition of MHD turbulence into different modes. As discussed in Section 3, it is clear that one might not be able to recover the usual centroids in the presence of absorption. As presented in Table 2, there is a range of scale where usual centroid asymptote can be obtained, and this range is set by the temperature of the turbulent cloud. Our results suggest that centroids work better for warm clouds than for cold ones in the presence of absorption. This can also be understood from equations (2) and (3). With increasing temperature (i.e. increasing $\beta_{\rm T}$), the intensity I_ν of an optically thick medium matches closer to that of an optically thin medium. Therefore, the usual centroids can be recovered for larger $\beta_{\rm T}$. Moreover, as shown in Fig. 3, there exist regimes of different scaling on R, and at some intermediate regime, the asymptote loses its dependence on velocity spectral index ν, thus entering a 'universal' regime. Note that Bertram et al. (2015) carried out the numerical simulations to study gas dynamics in molecular clouds using VCs. They observed a saturation of the spectral slope to value of -3, which corresponds to a scaling $\sim K^{-3}$ or equivalently R. Although their explanation was loosely based on VCA (LP04), our results show that this saturation exists not only in VCA, but also in centroids. It is also important to note that in the presence of self-absorption, the column density gets affected the same way as velocity, and therefore, obtaining MVC is still possible.

Originally, the centroids were developed for emission lines. However, our study in Section 4 extends UVC technique to study turbulence using absorption lines, which could be from the collection of point sources or from a spatially extended source. It is clear from our analysis that study of turbulence with absorption lines is possible with centroids if one considers the centroids of logarithm of intensity instead of intensity. Our results clearly show that if one considers sufficiently small lag, then one can still obtain the usual centroids scaling $R^{1+\nu}$. The range of lag R for which the usual centroid is obtained is set by width of the absorption window Δ and the thermal broadening $\beta_{\rm T}$. For larger $\beta_{\rm T}$, larger range of R shows the usual centroids scaling.

In terms of discussion on anisotropy, there are several important aspects that one can infer from our results. One of the important aspect is the issue of mode separation, i.e. identifying the composition of different MHD modes in a turbulent medium. With our result, it is clear that fast modes are easy to distinguish from Alfvén and slow modes due to two main reasons. First, fast modes show scaling in R different from Alfvén and slow modes. Secondly, the quadrupole to monopole ratio of fast mode is positive, while that of Alfvén and slow modes is negative. This means that iso-correlation contours are elongated along sky-projected magnetic field direction for Alfvén and slow modes, and orthogonal to it for fast modes. Note that KLP had similar findings on the distinctiveness of fast modes. With the present analysis, it is also clear that the separation of Alfvén and slow modes is challenging for two main reasons. First, the scaling on R shown by the two modes is the same, and secondly both modes have the same anisotropic power spectrum, which implies similar level of anisotropy of centroid structure.

As a novel suggestion, we presented study of centroids through interferometric data. The prime objects of study using centroids are turbulence in diffuse ISM of the Milky Way and other galaxies and in intergalactic gas in clusters of galaxies using multiwavelength single-dish and interferometric measurements. The advantage of interferometric study is that one just needs a few measurements rather than restoring the entire PPV cubes to be able to perform the studies.

9 COMPARISON BETWEEN VCA, VCS AND CENTROIDS

The VCA introduced in LP00 provided a new foundation for studying velocity and density turbulence by studying the changes of spectral slope of intensity fluctuations within velocity slices of PPV cubes. It was shown in LP00 that by choosing a sufficiently thin slice, one might be able to recover the velocity spectrum, whereas for sufficiently thick slice the velocity effects get washed away and only density spectrum can be recovered. The VCA was later extended in LP04 to account for the effects of self-absorption of emission lines. The results of LP04 suggest that in the presence of self-absorption, one might not be able to recover velocity spectrum, especially if the absorption is strong or the thermal broadening $\beta_{\rm T}$ is larger than the dispersion of the velocity field. In fact, it was shown in LP04 that one might observe a universal spectrum $P(K) \sim K^{-3}$ at some intermediate lag R, which corresponds to the spectrum measured in a number of studies (see examples in Lazarian 2009). The original formulation of VCA dealt only with power spectra, and this technique was further extended in KLP to study the anisotropies induced by magnetic field in a plasma. This study showed how the anisotropy of an underlying turbulent field maps to anisotropy of intensity fluctuations, and showed how the level of anisotropy depends on the Alfvén Mach number as well as the angle between LOS and mean magnetic field.

VC is another powerful technique to study turbulence. We believe that our extension of centroids to study turbulence in a media with self-absorption, as well as for absorption line significantly improves the value and power of this technique. In fact, we have also demonstrated how UVC can be used to study anisotropies of underlying turbulent field. The geometrical differences in construction of VCA and UVC are presented in Fig. 1.

We now compare the two techniques. The first important difference between the VCA and centroids is how thermal broadening $\beta_{\rm T}$ affects them. While VCA cannot recover velocity spectrum at scales R where $D_z(R) < \beta_{\rm T}$, centroids still work in this regime. This means that VCA does not work well for subsonic turbulence unless we use emission lines from subdominant slow massive species. Centroids, on the other hand, are not reliable for supersonic turbulence (see Esquivel et al. 2007). This is in contrast with VCA, which works well in this regime.

In the presence of self-absorption, the VCA and the UVC share some similarities. As shown in Section 3, in an optically thick medium one should expect a universal regime at some intermediate

Table 4. Comparison between centroids and VCA.

	Velocity centroids	VCA
Uses	LOS velocity-weighted intensity	Intensity
Best for	Subsonic turbulence	Supersonic turbulence
Scaling	$R^{1+\nu}$	$R^{1-\nu/2}$ or $R^{1+\nu_\rho-\nu/2}$ (thin slice[a]) $R^{1+\nu_\rho}$ (thick slice[b])

Notes. [a]For steep density $R^{1-\nu/2}$ dominates at small scales, while for shallow density $R^{1+\nu_\rho-\nu/2}$ dominates at small scales,
which allows one to get information about velocity spectrum in thin-slice limit.
[b]Velocity effects are washed away in the thick-slice limit, and only density spectrum can be recovered.

scales, where UVCs lose their ability to trace the underlying velocity field, same as in the VCA. Similarly, for $\nu < 2/3$ one should expect to see a thin-slice asymptote $R^{1-\nu/2}$ at some larger scales even in centroids as in the VCA. All the expected scaling from velocity effects in the presence of self-absorption is presented in Table 2 for both UVC and VCA. A brief comparison between VCA and UVC is also presented in Table 4.

Although the spectral index of a velocity field is an important parameter, it does not provide a complete picture of an underlying turbulent field. In fact, for a magnetized plasma, anisotropies are important descriptors of the underlying field. We have shown in Section 6 how the anisotropies of UVC structure function can be used to study the anisotropy of underlying turbulent field. This provides a complimentary tool to study anisotropies. As shown in this paper and in KLP, both VCA and UVC show similar traits in terms of anisotropy. First, the observed anisotropy in the thin-slice regime in VCA and in UVC both show a clear dependence on both Alfvén Mach number and the angle between the magnetic field and the LOS. Secondly, both studies demonstrate that the anisotropy due to fast modes is opposite to that due to Alfvén and slow modes. However, to obtain complete understanding of anisotropies, one still needs to correctly obtain the angle between magnetic field and the LOS, and the Alfvén Mach number and understand the characteristic difference between Alfvén and slow modes. We believe that these understandings can be significantly enhanced by combining VCA and centroids and through model fittings.

Besides VCA and centroids, VCS is another powerful technique to study turbulence. Unlike VCA and centroids, VCS exclusively uses data along the velocity coordinate (in particular in the Fourier space), and one does not need to spatially resolve the scale of turbulence under study. A major advantage of VCS is that only few independent measurements are enough to obtain information about the underlying velocity field (Chepurnov & Lazarian 2009).

We stress the importance of using different techniques such as VCA, VCS and centroids when studying multiphase ISM, e.g. H I and Hα. While VCA and VCS do not work well for gas components with large thermal broadening $\beta_{\rm T}$ due to thermal dampening of the fluctuations,[4] centroids work well for both hot and cold components at least as long as the turbulence is subsonic. Therefore, synergy of different techniques is advantageous, as these techniques have their own advantages.

10 PRACTICAL ASPECTS OF STUDIES OF TURBULENCE USING CENTROIDS

In this section, we discuss some of the practical aspects of studying turbulence with centroids. First, when centroids are used to study turbulence in external galaxy, one must consider the contribution from galactic rotation to the LOS velocity, and thus to the centroids. Several methods are available to remove this contribution through the estimation of galactic rotation curve (see for e.g. Miesch & Bally 1994; Miesch et al. 1999; Dutta 2016). In this paper, we have assumed that coherent motions such as rotations have been subtracted from the PPV data. Our approach has benefited from the formulation of centroids in PPV space which can assume that such cleaning steps have been done before correlation studies.

Centroids are most suitable for subsonic turbulence. One of the candidates for objects of study for such turbulence is the clusters of galaxies. An example of a cluster suitable for turbulence studies would be a nearby Coma cluster, where a potential cause of turbulence is an ongoing merger activity (ZuHone, Markevitch & Zhuravleva 2016). The observational study of turbulence could be carried out with the data using new-generation X-ray observatories such as *Astro-H* (Takahashi et al. 2012). Some of the practical aspects of studying turbulence have been presented in ZuHone et al. (2016), where they use normalized centroids to numerically test the ability of *Astro-H* to constrain various parameters (such as injection scale, Mach number). *Astro-H*, for instance, has capability to obtain LOS velocities as well as velocity dispersion with a spectral resolution of the order of km s^{-1}. Centroids are suitable when a good spatial coverage is available, otherwise a complimentary technique to study turbulence when such coverage is unavailable is VCS. VCS can be used with heavier species (such as Fe) in clusters, for which the thermal broadening $\beta_{\rm T}$ is small. The advantage of VCS is that only few spectral measurements are enough to obtain turbulence spectra, and one does not even need a good spectral resolution to study turbulence.

X-ray observations are used to measure velocity and intensity profiles in such clusters, but X-ray observatories often have limited spectral resolution. None the less, one should still be able to use centroids as long as the dynamical range width ΔV_i of an instrument over which they are sensitive to signal is larger than the spread $\Delta V_0 = \sqrt{D_z(S) + 2\beta_{\rm T}}$ of the signal. Zhuravleva et al. (2012, hereafter ZX12) commented that with an energy resolution of 5 eV and angular resolution of 1.7 arcmin, one should be able to measure the line profiles in Perseus cluster (where rms velocity of gas motions is $\sim$300 km s^{-1}) with 90 per cent confidence level with the measurement time of $\sim 4 \times 10^5$s.

Thermal broadening can put an important limitation on one's ability to obtain velocity dispersion, as the measured width of the line is affected by thermal motions of emitters. However, as noted in ZX12, thermal broadening is not important especially when one considers heavy species such as Fe. It was discussed in ZX12 that for instruments such as *Astro-H* with energy resolution of 7 eV at 6.7 keV line width of Fe, and at gas motions of speed $\sim$400 km s^{-1}, thermal broadening is unlikely to be significant.

[4] One strategy to use VCA and VCS in a hot medium is to use emission lines from heavy species such as Fe.

An important limitation of an instrument is its finite spatial resolution. A finite diagram θ_0 of an instrument introduces uncertainty $\delta R \sim \theta_0$ in the scales. Therefore, one should study centroids at scales $R > \theta_0$. Moreover, if the spatial resolution of the telescope is not good enough, then in the presence of self-absorption, one cannot see the turbulence induced statistics, but only the universal $\sim R$ regime. To put this in perspective, we take a specific example of an instrument with 1.7 arcmin angular resolution, which is used to study Perseus cluster, which is at a distance of 72 Mpc. With this resolution, only lags $R > 20$ kpc can be studied to obtain turbulence spectra.

The effect of instrumental noise has been discussed in detail in Dickman & Kleiner (1985, hereafter DK85) and Miesch & Bally (1994), where it was shown that actual correlations are underestimated in the presence of instrumental noise. DK85 suggested to apply a constant multiplicative factor to account for noise contributions at non-zero lag.

The studies of the effects of noise in DK85 were carried out for normalized centroids. Here, we apply their study for unnormalized centroids. In the presence of noise, the centroids structure function can be written as

$$\mathcal{D}_N(R) = \mathcal{D}(R) + 2\sigma_N^2, \tag{75}$$

where $\mathcal{D}(R) \equiv \left\langle [C(\boldsymbol{X}_1 + \boldsymbol{R}) - C(\boldsymbol{X}_1)]^2 \right\rangle$, σ_N^2 is the variance due to noise. Since $\mathcal{D}(R) \propto R^n$, where $n > 0$ is some index, it is clear that at extremely short scales, the centroid structure function can be corrupted by the noise. To estimate σ_N, we decompose the measured spectral intensity $I_{v,i}$ in a velocity channel i into contributions from true emissions $I^s_{v,i}$ and contributions from noise $\delta I_{v,i}$, so that the centroids can be written as

$$C = \sum_{i=1}^{N} I^s_{v,i} v_i + \sum_{i=1}^{N} \delta I_{v,i} v_i. \tag{76}$$

The noise in two different spectroscopic channels is uncorrelated, and thus satisfies the constraints $\langle \delta I_{v,i} \delta I_{v,j} \rangle = \delta I^2$ for $i = j$ and 0 otherwise. From equation (76), it is clear that the error in centroids due to noise is $\delta C = \sum_{i=1}^{N} \delta I_{v,i} v_i$, and therefore the dispersion due to noise is given by

$$\sigma_N^2 = \delta I^2 \sum_{i=1}^{N} v_i^2. \tag{77}$$

As shown in DK85, for large N, $\sum_{i=1}^{N} v_i^2 \approx \Delta^2 N^3/12$, where Δ is the width of the spectroscopic channel. Using equation (77), one finally obtains

$$\sigma_N^2 \approx \frac{\Delta^2 N^3 \delta I^2}{12}. \tag{78}$$

With this, the lags at which turbulence can be studied in the presence of noise can be estimated by considering scales for which $\mathcal{D}(R) > 2\sigma_N^2$. Restoring dimensional pre-factors in the expression for $\mathcal{D}(R)$, we obtain

$$\frac{R}{S} > \left(\frac{\Delta^2 N^3}{6 D_z(S)} \frac{\delta I^2}{\bar{I}^2} \right)^{\frac{1}{1+v}}, \tag{79}$$

where $\bar{I}$ is the mean spectral intensity in a spectroscopic channel. In the case when background count per second in a spectral bin is given by n_b, the actual emission count per second in a spectral bin by n_a, one can write

$$\frac{\delta I^2}{\bar{I}^2} = \frac{n_a + n_c}{n_a^2 t}, \tag{80}$$

where t is the measurement time. Equations (79) and (80) tell us that in the presence of noise, we can still study turbulence albeit not at extremely short scales. Moreover, the effect of noise can be reduced by increasing instrument time, as seen from equation (80). It is important to note that to reduce the effects of noise, one should use a velocity window which is just wide enough to account for major signals.

11 DISCUSSION

11.1 Foundations of the technique

In this paper, we improve the understanding of centroids by studying unnormalized centroids in the presence of self-absorption, carrying out absorption line study and studying the effects of anisotropies in MHD turbulence. Unlike the past works, we explicitly use PPV space for absorption line study and study of self-absorption. This work shows the strength and usefulness of the PPV space formalism developed in LP00.

In the view of modern understanding of MHD turbulence (see Beresnyak & Lazarian 2015 for a review), we study anisotropy of centroid correlation through explicit calculations in mode-by-mode basis. Theoretical and numerical research (GS95; Lithwick & Goldreich 2001; Cho & Lazarian 2002, 2003; Kowal & Lazarian 2010) suggest that the MHD turbulence can be viewed as a superposition of the cascades of Alfvén, slow and fast modes. The statistical properties of these cascades in the global frame of reference were obtained in LP12 for the magnetic fields, while similar study was carried out in KLP for the velocity field. In particular, KLP studied turbulence anisotropies by making use of the VCA technique.

The variations of spectral indexes m of power spectrum for the velocity field, $P(k) \sim k^{-m}$, are rather limited. The range of m is likely to be between $m = 3/2$ and $m = 2$, with $m = 3/2$ expected for acoustic turbulence and $m = 2$ for shocks. Numerical simulations in Kritsuk et al. (2009) and Kowal & Lazarian (2010) indicate that this range might be even more restrictive from approximately $m = 5/3$ to somewhat shallower than $m = 2$. The latter is present for high sonic Mach numbers. Non-ideal MHD effect such as partial ionization is not expected to change the velocity spectral index down to the ion–neutral damping scales. The reported spectral index $m = 4$ in the viscosity-damped regime of turbulence (see Lazarian, Vishniac & Cho 2004) is probably too steep to be seen observationally. On the other hand, spectral index of density changes from 5/3 to much more shallow values as discussed in Kowal, Lazarian & Beresnyak (2007). Again, partial ionization is not expected to significantly affect the results at scales where the ions and neutrals are coupled.

11.2 Model assumptions

In this paper, we adopted several model assumptions to make our analysis possible. One of the main assumptions is that the fluctuations are Gaussian. This assumption is satisfied by the velocity field to an appreciable degree (see Monin et al. 1975). We do not make any assumption about Gaussianity of density field in the case when the turbulent medium is optically thin, as well as for absorption line studies, but we use Gaussian approximation for PPV space density to understand the main effects of self-absorption.

While LE03 derived a general expression for centroid structure function keeping in mind that velocity and density might be correlated, we assumed that they are not. In fact, Esquivel et al. (2007) investigated the effects of density velocity correlation and showed that this correlation is not important if $\sigma_\rho/\rho_0 \lesssim 1$. If this condition

is not fulfilled, one should develop a model of density–velocity, perhaps basing on numerical simulation, correlation to retrieve full information from the centroids.

Our analysis of centroid anisotropy was based on the decomposition of MHD turbulence into Alfvén, slow and fast modes. This decomposition is reasonable only when the coupling between the modes is marginal. Cho & Lazarian (2002) showed that the degree of coupling between different modes to be moderate as long as the sonic Mach number is not very high. Since the main regime where centroids are reliable is subsonic turbulence, this condition may not be restrictive for our purpose.

11.3 New power of centroids

This paper improves the usefulness of the UVC technique by providing an analytical description of the technique in the presence of self-absorption as well as for the absorption line study. We believe that our study will be complimentary to the study in LP04, where effects of self-absorption were studied in the context of VCA. We also extend the ability of the centroids technique to study magnetization of a media and direction of the magnetic field, and explored the possibility of separating contributions of Alfvén, slow and fast modes. The separation of mode is important because different modes have different astrophysical impacts. As an example, Alfvén modes are essential for magnetic field reconnection (Lazarian & Vishniac 1999, see also Lazarian et al. 2015 and references therein), superdiffusion of cosmic rays (Lazarian & Yan 2014), etc. On the other hand, fast modes are important for resonance scattering of cosmic rays (Yan & Lazarian 2002). The possible ability of centroids to obtain the relative contribution of these different modes complements this ability for the techniques introduced in LP12 and LP16 for synchrotron data and in KLP for spectroscopic data.

11.4 Centroids and other techniques

In this paper, we studied centroids by extensively making use of PPV space formalism. We have also discussed and compared centroids with the VCA and VCS, the techniques that were developed also by using PPV space formalism. Centroids have been used to analytically study anisotropies in this paper, while anisotropies were studied using VCA in KLP. Another technique called PCA (see Brunt & Heyer 2002) can also be used to study turbulence anisotropies. However, unlike the centroids and VCA, it is not easy to quantify PCA using PPV data. Nevertheless, recent studies have shown the sensitivity of PCA to the phase information (Correia et al. 2016), although the trend is not yet clear.

Another important technique to study turbulence using velocity slice of PPV space is the spectral correlation function (SCF; see Rosolowsky et al. 1999). The SCF is very similar to VCA if one removes the adjustable parameters from SCF. In fact, both SCF and VCA measure correlations of intensity in velocity slices of PPV, but the SCF treats outcomes empirically. There also exist numerous techniques identifying and analysing clumps and shells in PPV (see Stutzki & Guesten 1990; Houlahan & Scalo 1992; Williams, De Geus & Blitz 1994; Pineda et al. 2006; Ikeda, Sunada & Kitamura 2007).

Besides the VCA and centroids, there are also some other techniques to study sonic and Alfvén Mach numbers. Some of these techniques include the so-called Tsallis statistics (see Esquivel & Lazarian 2010; Tofflemire, Burkhart & Lazarian 2011), bi-spectrum (see Burkhart et al. 2009), genus analysis (see Chepurnov et al. 2008), etc. Using different available techniques allows one to obtain a comprehensive picture of MHD turbulence.

12 SUMMARY

On the basis of the analytical theory of the intensity fluctuations in the PPV space developed in the earlier works (LP00, LP04, LP08, KLP), we provided the analytical description of the statistics of fluctuations measured by VCs. Our definition of centroids follows that in LE03 and differs from the traditionally used by the absence of the normalization by intensity. While the normalization makes analytical studies really prohibitive, it was shown in numerical studies in Esquivel & Lazarian (2005) to be of no significance for restoring underlying velocity statistics. Therefore, we use UVCs (Esquivel & Lazarian 2005, see Table 1). Our results can be briefly summarized as follows.

(i) We proved the complementary nature of turbulence studies with VCs and the VCA. Both techniques can measure turbulence spectra and anisotropy. While centroids are reliable for study of subsonic turbulence statistics, one has to use only heavier species, e.g. metals in hydrogen gas, to study subsonic turbulence using VCA. We showed how one can use centroids to study anisotropies of different MHD modes.

(ii) Analytical expressions for UVC structure function are obtained in the presence of emission lines and self-absorption as well as for the absorption lines. In the presence of self-absorption, new scalings of correlation of fluctuations measured by UVC at different scales are reported. Similar to the VCA, for a range of scales, the UVC correlations are shown to exhibit universal scaling, thus losing the information of the velocity spectra.

(iii) For absorption line, we suggest to construct UVC as LOS-velocity-weighted logarithm of intensity, and focus on the wings where absorption lines are not saturated. We termed thus defined centroid as restricted velocity centroid (RVC) (see equation 32) and showed that at sufficiently small lags it exhibits the usual centroids scaling. RVCs open a new way of probing astrophysical turbulence. Both turbulence statistics and turbulence anisotropies can be studied using RVCs.

(iv) Analytical expression of UVC structure function and anisotropy level for sub-Alfvénic turbulence are derived. These expressions are used to study the anisotropy arising from three MHD modes: Alfvén, fast and slow. It is shown that the quadrupole to monopole ratio of fast mode is positive, while it is negative for Alfvén and slow modes. In other words, isocorrelation contours are elongated along sky-projected magnetic field direction for Alfvén and slow modes, and orthogonal to it for fast modes, which is the same as what VCA predicts (see KLP).

(v) Self-absorption of the radiated emission does not preclude anisotropy studies with UVCs, MVCs and RVCs. Our study suggests that at sufficiently short lag R, one will observe the same level of anisotropy as that of optically thin centroids, while at larger scales the anisotropy level decreases to the level of thin-slice regime of VCA.

(vi) Interferometric output can be used to directly measure spectra and anisotropy of the UVC statistics using the Fourier components of the intensity distribution that are available with interferometers. This considerably simplifies such measurements, as there is no necessity to restore the image of the turbulent volume. Instead, having a few of these Fourier components is sufficient to get both spectra and anisotropy of turbulence.

ACKNOWLEDGEMENTS

DK and DP thank the Institut Lagrange de Paris, a LABEX funded by the ANR (under reference ANR-10-LABX-63) within the Investissements d'Avenir programme under reference ANR-11-IDEX-0004-02. AL acknowledges the NSF grant AST 1212096 and Center for Magnetic Self Organization (CMSO). He also acknowledges Institut Astrophysique du Paris and Institut Lagrange de Paris for hospitality during his visit.

REFERENCES

Ballesteros-Paredes J., Klessen R., Mac Low M.-M., Vazquez-Semadeni E., 2007, Protostars and Planets V. Univ. Arizona Press, Tucson, AZ, p. 63
Beresnyak A., Lazarian A., 2015, Magnetic Fields in Diffuse Media. Springer-Verlag, Berlin, p. 163
Bertram E., Konstandin L., Shetty R., Glover S. C., Klessen R. S., 2015, MNRAS, 446, 3777
Brandenburg A., Lazarian A., 2013, Space Sci. Rev., 178, 163
Brunt C. M., Heyer M. H., 2002, ApJ, 566, 276
Burkhart B., Falceta-Gonçalves D., Kowal G., Lazarian A., 2009, ApJ, 693, 250
Burkhart B., Lazarian A., Ossenkopf V., Stutzki J., 2013, ApJ, 771, 123
Burkhart B., Lazarian A., Leão I., De Medeiros J., Esquivel A., 2014, ApJ, 790, 130 (BX14)
Chepurnov A., Lazarian A., 2009, ApJ, 693, 1074
Chepurnov A., Lazarian A., 2010, ApJ, 710, 853
Chepurnov A., Gordon J., Lazarian A., Stanimirovic S., 2008, ApJ, 688, 1021
Chepurnov A., Burkhart B., Lazarian A., Stanimirovic S., 2015, ApJ, 810, 33
Cho J., Lazarian A., 2002, Phys. Rev. Lett., 88, 245001
Cho J., Lazarian A., 2003, MNRAS, 345, 325
Cho J., Vishniac E. T., 2000, ApJ, 539, 273
Cho J., Lazarian A., Vishniac E. T., 2002, ApJ, 564, 291
Cho J., Lazarian A., Vishniac E. T., 2003, in Falgarone E., Passot T., eds, MHD Turbulence: Scaling Laws and Astrophysical Implications. Springer-Verlag, Berlin, p. 56
Correia C., Lazarian A., Burkhart B., Pogosyan D., Medeiros J. R. D., 2016, ApJ, 818, 118
Dickman R., Kleiner S., 1985, ApJ, 295, 479 (DK85)
Dutta P., 2016, MNRAS, 456, L117
Elmegreen B. G., Scalo J., 2004, ARA&A, 42, 211
Esquivel A., Lazarian A., 2005, ApJ, 631, 320
Esquivel A., Lazarian A., 2010, ApJ, 710, 125
Esquivel A., Lazarian A., 2011, ApJ, 740, 117 (EL11)
Esquivel A., Lazarian A., Horibe S., Cho J., Ossenkopf V., Stutzki J., 2007, MNRAS, 381, 1733
Federrath C., 2013, MNRAS, 436, 3167
Federrath C., Klessen R. S., 2012, ApJ, 761, 156
Goldreich P., Sridhar S., 1995, ApJ, 438, 763 (GS95)
Heyer M. H., Peter S. F., 1997, ApJ, 475, 173
Higdon J., 1984, ApJ, 285, 109
Houlahan P., Scalo J., 1992, ApJ, 393, 172
Ikeda N., Sunada K., Kitamura Y., 2007, ApJ, 665, 1194
Kandel D., Lazarian A., Pogosyan D., 2016, MNRAS, 461, 1227 (KLP)
Kleiner S., Dickman R., 1985, ApJ, 295, 466
Kowal G., Lazarian A., 2010, ApJ, 720, 742
Kowal G., Lazarian A., Beresnyak A., 2007, ApJ, 658, 423
Kritsuk A. G., Ustyugov S. D., Norman M. L., Padoan P., 2009, J. Phys.: Conf. Ser., 180, 012020
Lazarian A., 2009, Space Sci. Rev., 143, 357
Lazarian A., Esquivel A., 2003, ApJ, 592, L37 (LE03)
Lazarian A., Pogosyan D., 2000, ApJ, 537, 720 (LP00)
Lazarian A., Pogosyan D., 2004, ApJ, 616, 943 (LP04)
Lazarian A., Pogosyan D., 2006, ApJ, 652, 1348 (LP06)
Lazarian A., Pogosyan D., 2008, ApJ, 686, 350 (LP08)
Lazarian A., Pogosyan D., 2012, ApJ, 747, 5 (LP12)
Lazarian A., Pogosyan D., 2016, ApJ, 818, 178 (LP16)
Lazarian A., Vishniac E. T., 1999, ApJ, 517, 700
Lazarian A., Yan H., 2014, ApJ, 784, 38
Lazarian A., Pogosyan D., Vázquez-Semadeni E., Pichardo B., 2001, ApJ, 555, 130
Lazarian A., Pogosyan D., Esquivel A., 2002, in Taylor A. R., Landecker T. L., Willis A. G., eds, ASP Conf. Ser. Vol. 276, Seeing Through the Dust: The Detection of HI and the Exploration of the ISM in Galaxies. Astron. Soc. Pac., San Francisco, p. 182
Lazarian A., Vishniac E. T., Cho J., 2004, ApJ, 603, 180
Lazarian A., Eyink G., Vishniac E., Kowal G., 2015, Phil. Trans. R. Soc. A, 373, 20140144
Lithwick Y., Goldreich P., 2001, ApJ, 562, 279
Mac Low M.-M., Klessen R. S., 2004, Rev. Mod. Phys., 76, 125
McKee C. F., Ostriker E. C., 2007, ARA&A, 45, 565
Maron J., Goldreich P., 2001, ApJ, 554, 1175
Miesch M. S., Bally J., 1994, ApJ, 429, 645
Miesch M. S., Scalo J., Bally J., 1999, ApJ, 524, 895
Monin A. S., Yaglom A. M., Lumley J. L., eds 1975, Statistical Fluid Mechanics: Mechanics of Turbulence, Vol. 2. MIT Press, Cambridge, MA
Montgomery D., Turner L., 1981, Phys. Fluids, 24, 825
Münch G., Wheelon A. D., 1958, Phys. Fluids, 1, 462
O'dell C., Castaneda H. O., 1987, ApJ, 317, 686
Padoan P., Juvela M., Kritsuk A., Norman M. L., 2009, ApJ, 707, L153
Pineda J. E., Caselli P., Goodman A. A., Rosolowsky E., Foster J. B., 2006, BAAS, 209, 5505
Rosolowsky E. W., Goodman A. A., Wilner D. J., Williams J. P., 1999, ApJ, 524, 887
Salim D. M., Federrath C., Kewley L. J., 2015, ApJ, 806, L36
Shebalin J. V., Matthaeus W. H., Montgomery D., 1983, J. Plasma Phys., 29, 525
Stutzki J., Guesten R., 1990, ApJ, 356, 513
Takahashi T., Murray S. S., den Herder J.-W. A., eds 2012, Proc. SPIE Conf. Ser. Vol. 8443, Space Telescopes and Instrumentation 2012: Ultraviolet to Gamma Ray. SPIE, Bellingham, p. 84431Z
Takamoto M., Lazarian A. 2016, ApJL, preprint (arXiv:1610.01373)
Tofflemire B. M., Burkhart B., Lazarian A., 2011, ApJ, 736, 60
Williams J. P., De Geus E. J., Blitz L., 1994, ApJ, 428, 693
Yan H., Lazarian A., 2002, Phys. Rev. Lett., 89, 281102
Zhuravleva I., Churazov E., Kravtsov A., Sunyaev R., 2012, MNRAS, 422, 2712 (ZX12)
ZuHone J., Markevitch M., Zhuravleva I., 2016, ApJ, 817, 110

APPENDIX

Table A1. List of notations used in this paper.

Parameter	Meaning	First appearance
$\boldsymbol{x}$	3D position vector	Equation (3)
$\boldsymbol{X}$	2D position vector	Equation (1)
$\boldsymbol{r}$	3D separation $\boldsymbol{x}_2 - \boldsymbol{x}_1$	Equation (8)
$\boldsymbol{R}$	2D separation $\boldsymbol{X}_2 - \boldsymbol{X}_1$	Equation (8)
$\rho_{\rm s}(\boldsymbol{X}, v)$	Density of emitters in the PPV space	Equation (2)
$\Phi(v)$	Maxwell's distribution function	Equation (3)
$\beta_{\rm T}$	Thermal broadening	Equation (11)
$\xi_\rho(\boldsymbol{x})$	Density correlation function	Equation (8)
$D_z(\boldsymbol{r})$	LOS-projected velocity structure function	Equation (11)
$d_\rho(\boldsymbol{r})$	Density structure function	Equation (15)
S	Size of a turbulent cloud	Equation (8)
$v_{\rm ab}$	Velocity cut-off introduced by self-absorption	Equation (25)
$\tau(\boldsymbol{X}, v)$	Optical depth	Equation (28)
Δ	Characteristic width of the window in the absorption line study	Equation (32)
$\hat{\lambda}$	Direction of the mean magnetic field	Equation (40)
$a_{\boldsymbol{k}}$	Random amplitude of a mode	Equation (40)
$\hat{\xi}_{\boldsymbol{k}}$	Direction of allowed displacement in a plasma	Equation (40)
$\mathcal{A}(k, \hat{\boldsymbol{k}} \cdot \hat{\lambda})$	Power spectrum of a mode	Equation (40)
$\cos\phi$	2D angle between sky-projected $\boldsymbol{r}$ and sky-projected $\hat{\lambda}$	Equation (46)
$\cos\gamma$	Angle between LOS and symmetry axis	Equation (54)
$\mathcal{D}_n(R)$	Multipole moment of centroid structure function	Equation (48)

This paper has been typeset from a TEX/LATEX file prepared by the author.